Journal of Power Sources 396 (2018) 691–709

Contents lists available at ScienceDirect

Journal of Power Sources

journal homepage: www.elsevier.com/locate/jpowsour

Review article

Economic implications of lithium ion battery degradation for Vehicle-to-Grid (V2X) services

Andrew W. Thompson[a,b,*]

[a] RITM Lab, University of Paris-Sud 11, Faculté Jean Monnet, 54 Boulevard Desgranges, 92330, Sceaux, France
[b] Institut VEDECOM, 77 Rue des Chantiers, 78000, Versailles, France

HIGHLIGHTS

- Comprehensive review of the economic implications of Li-ion battery degradation.
- Calendar Aging is dominant life reducing factor in vehicular applications.
- Battery Degradation Cost is predominately time and temperature dependent.
- Economic analyses of degradation cost should be informed by battery lifetime models.
- V2X services can prolong battery life but cost effectiveness is chemistry dependent.

ARTICLE INFO

Keywords:
Vehicle-to-Grid (V2G)
Ancillary Services
Lithium-ion battery degradation costs
Lithium-ion battery degradation modeling

ABSTRACT

Electric and Plug-in Hybrid Electric Vehicles are a promising sustainable mobility alternative due to their low emissions impact and the rapidly falling production costs of Li-ion batteries. To lower total vehicle ownership costs, Vehicle-to-Grid/Building/Home (V2X) services aim to derive additional value from the battery asset through dynamic or bi-directional charge control to provide benefits to the electric grid or to reduce/flatten/shift peak energy consumption of buildings. Battery State of Health (SOH) is impacted through reduction of total capacity and/or increase in internal impedance due to various degradation mechanisms which collectively result in Calendar Aging and Cycling Aging behaviors. At moderate temperatures, Calendar Aging is the dominant factor and this understanding paired with the fact that most vehicles are immobile more than 90% of the time, implies that the battery management strategy while at rest will bound lifetime. Evidence suggests that V2X could prolong battery life through integration with optimized management algorithms and that cost effective V2X services may be dependent on battery chemistry. Therefore economic analyses of battery assets should contain sufficient electrochemical detail to account for chemistry specific degradation behavior.

1. Introduction

The transportation sector accounts for around 25% of global energy-related carbon emissions of which light-duty passenger vehicles account for over half and their impact is expected to grow in the coming years [1,2]. It is clear, that to achieve the necessary carbon emission reductions agreed upon in the Paris Climate Accords there must be a substantial contribution from the transport sector [3]. Replacement of light-duty vehicles with Electric Vehicles (EV) and Plug-in Hybrid Electric Vehicles (PHEV) offers a promising alternative to take advantage of synergies between the Energy and Transport sectors, yet their effectiveness as a solution depends on a decarbonized electric grid and the availability of cost competitive battery technology.

Lithium-ion technology provides the highest specific power and specific energy over other commercial battery and storage types [4]. Battery costs have been reduced by a factor of four since 2008 and are set to decrease further; additionally, energy density of lithium ion batteries has increased substantially as seen in Figure S1 in the Supplementary Materials. Over the course of seven years from 2009 to 2015, PHEV batteries experienced an almost 400% increase in energy density [1]. As such, Lithium-ion technology offers the most promising battery solution for the near future.

While PHEVs and other hybrid topologies are already well established in the market, key barriers to large scale EV market penetration include battery costs and vehicle range, both areas where recent technology developments provide encouraging signs. Evidence suggests that

* Institut VEDECOM, 77 Rue des Chantiers, 78000, Versailles, France.
E-mail address: andrew.thompson@vedecom.fr.

https://doi.org/10.1016/j.jpowsour.2018.06.053
Received 11 April 2018; Received in revised form 3 June 2018; Accepted 11 June 2018

EVs may reach price parity with Internal Combustion Engine (ICE) vehicles by 2022 [5]. There are several ongoing approaches to these barriers EV adoption.

The first approach is to lower the cost of battery packs thus lowering the Total Cost of Ownership (TCO) of EVs. This strategy is noted as the "Tesla approach", which aims to exhaust economies of scale while improving manufacturing techniques and drastically reducing shipping costs by assembling battery packs in-house.

The second is to invest in research and development of new battery chemistries and new technology. Research is directed towards the development of longer lasting and safer cells with greater energy density, thus lowering per kWh costs. This includes experimentation with new additives in electrolyte and cathode materials for longer lasting Li-ion cell chemistry [6–10]. New technologies include Lithium Sulfur (Li-S) and Lithium Air (Li-O2) battery configurations, the use of solid electrolytes over organic liquid electrolytes for the creation of Solid State Batteries (SSB), and incorporation of new anode materials such as Silicon and Titanate [11–16].

The third approach is related to developing more intelligent Battery Management Systems (BMS) to allow for smaller batteries to satisfy the same mobility demands, thus lowering the TCO of EVs through decreased capacity requirements and the additional cost savings from reduction in vehicle weight [17,18].

The fourth approach, which is the focus of this review, is to develop new revenue streams to offset the high initial cost of EVs through participation in energy markets and provision of grid services, or through diminishing the energy burden of buildings or homes. Vehicle-to-Grid (V2G), Vehicle-to-Building (V2H), Vehicle-to-Home (V2H), Vehicle-to-Load (V2L), and Vehicle-to-Vehicle (V2V) collectively denoted as V2X services, aim to derive additional value from the battery asset during times of non-use in the primary objective of mobility [19].

1.1. V2X Services

Unlike the standard load demands that EV battery packs which are designed for mobility-only undergo, the resultant load demand from a V2X product is inherently dependent on the underlying energy service. Thus V2X should be considered an umbrella term under which several distinct energy services can be provided therefore a generalized V2X load profile does not exist. It is however possible to develop load profiles for individual V2X products depending on the connection topology (V2G, V2B, V2H, V2L, and V2V) and the energy service being provided (Frequency Regulation, Energy Arbitrage, Emergency Back-up Power, etc.) as elaborated in the following sections 1.1.1 and 1.1.2.

V2X can be generalized into energy based products and power based products. Bulk energy transfer products such as performing V2G energy arbitrage (charging/buying electricity during times of low energy prices and discharging/selling during periods of high energy prices), providing V2G spinning reserves (bulk energy discharge or dynamically altering charge rate in response to grid requirements), acting as a Demand Response (DR) resource, or serving as emergency back-up power (V2H/V2B), all result in similar load profiles in that a large energy throughput is required which translates to long periods of charging or discharging for a vehicle battery. Frequency of use, daily timing, and utilization rates for each service will differ however and are further elaborated in Section 5.2.2. Power products however (most notably V2G frequency regulation) where fast response time is crucial will result in significantly less energy exchange as the inherent energy service is charge/discharge flexibility. Fig. 1 below is a visual overview the various V2X topologies which shows interaction type with grid operators and operating location either in the High Voltage (HV), Medium Voltage (MV) or Low Voltage (LV) networks [20]. Note that a V2B topology is similar to the V2H pictured with the addition of multiple vehicles or a fleet which implies a more sophisticated building energy management system but the concept is the same. Additionally the V2L and V2V topologies are similar.

1.1.1. Vehicle-to-Grid (V2G)

Vehicle-to-Grid services relate to utilizing an electric vehicle battery as either a Distributed Energy Resource (DER) or as storage for the electric grid. V2G is envisioned to predominately provide Ancillary Services due to the inherent characteristics of an EV resource which include a near-instantaneous response time and limited energy capacity. Four potential products exist in current energy markets for V2G services: Spinning Reserves, Peak Power Shaving (also known as Energy Arbitrage), Frequency Regulation (or Regulation Reserves), and Demand Response [21–23].[1] While the other Ancillary Services have been shown to be economically competitive in certain situations, Frequency Regulation has been identified as the first most promising and lucrative market due to its inherent characteristics which include a seconds-time interval response requirement and a low net energy requirement with relatively high market prices [21,24]. Figure S2 in the Supplementary Materials is an example frequency regulation load profile which compares PJM's Reg A (Ordinary Regulation, net energy variable) and Reg D (Fast Response Regulation, net energy neutral) signals and their impact on battery State-of-Charge (SOC) of a Battery Energy Storage System (BESS) [25]. Due to the inherent nature of the usage case (high frequency charging/discharging load profile) a low net energy exchange and a shallow charge/discharge cycle results which is known to be less detrimental to batteries as will be explained in Section 3.

The US Frequency Regulation Market is highly volatile which often experiences price spikes of over 100 ($/MW-h) while typical prices can range from 5 to 65 ($/MW-h) depending on the regional market. Market revenue has grown from under $20 million in 2009 to over $380 million in 2014; however Frequency Regulation is a relatively shallow market with an average capacity requirement of 410 MW [26]. Due to these characteristics, it is envisioned that V2G would likely provide Frequency Regulation first while descending the technology learning curve until market saturation and later expand into larger markets.

Lazard's Levelized Cost of Storage (LCOS) analysis has identified that non-subsidized stationary lithium-ion Battery Energy Storage Systems (BESS) on the high-end have already achieved cost competitiveness with conventional gas peaker plants for Frequency Regulation services as of 2015, with projected 5-year developments likely to lead to full cost competitiveness across all installations [27]. Subsequent analysis showed an estimated 5-year capital cost reduction of Lithium-ion Batteries between 26 and 29% [28]. The question remains however, if lithium ion technology in an electric or plug-in hybrid vehicle configuration can deliver a similar value proposition.

Current Ancillary Service regulation requires a minimum capacity to bid into the market ranging from 100 kW–5 MW [29,30]. These rules constitute a barrier to entry for small capacity resources yet reflect the reality that only significantly large loads are economically worth controlling during real-time grid operation. While an EV charging at even the lowest L1 charging power will draw roughly 2 kW which would double the instantaneous power requirement of a household, it is a negligible amount in the context of the transmission grid. However, 100 EVs charging simultaneously would be well above the minimum capacity requirement regardless of the charging level used. As such, V2G is likely to be employed by an aggregator which intelligently coordinates several distributed resources to provide grid-significant capacity [31,32].

[1] These Ancillary Service products are from US energy market definitions. In Europe these Ancillary Services have recently been redefined as Frequency Containment Reserves (FCR), Frequency Restoration Reserves (FRR), and Replacement Reserves (RR) in efforts to harmonize the various definitions across EU Member States [112]. Other international markets may have additional definitions for Ancillary Services.

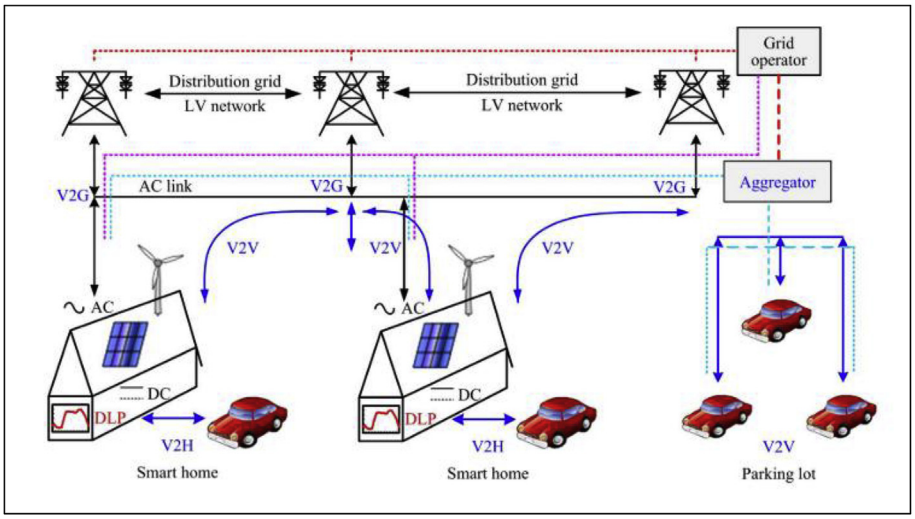

Fig. 1. Overview of various V2X topologies (readers are referred to the web version of this article for color). The blue dotted line indicates aggregated control while the purple dotted line indicates individual interaction with the grid operator. The red dotted lines indicate interaction with the grid operator at the Medium Voltage (MV) and High Voltage (HV) networks. This framework shows that V2H (V2B) and V2V (V2L) operate at the Low Voltage (LV) network mostly behind-the-meter while V2G could operate both in the LV and MV network depending on aggregation size and type. Interested readers are referred to the original source which additionally provides a thorough overview of V2X integration with the rest of the electric grid at the various connection points [20]. (For interpretation of the references to color in this figure legend, the reader is referred to the Web version of this article.)

1.1.2. Vehicle-to-Building (V2B), Vehicle-to-Home (V2H), Vehicle-to-Load (V2L), and Vehicle-to-Vehicle (V2V)

Vehicle-to-Building (V2B) or Vehicle-to-Home (V2H) relate to employing an EV or PHEV as a means to optimize energy consumption and to limit overall energy usage by reducing, flattening, or shifting peak energy consumption in either a building or a home. Vehicle-to-Load (V2L) or Vehicle-to-Vehicle (V2V) typically relate to using a vehicle as emergency back-up power or as a mobile energy source. Several research projects have focused on employing EV fleets with rooftop solar sources and have found there are many interesting value propositions for both homes and building integration [33–36]. Additionally [37], found that energy storage paired with buildings will result in reduced load variability along with several other derivative benefits such as capital cost deferment, reduction of carbon emissions, and reduction of operation costs for both grid operators and building managers.

There has also been investigation into using EV and PHEVs for reactive power balancing in either a V2B or V2H topology to improve the load power factor thus improving power quality and reducing losses [38]. Power Factor improvement provided by V2B or V2H would mitigate the need for high capital cost capacitor banks which are still in use in industrial buildings today [39,40].

V2H/V2B topologies avoid the infrastructure and tariff problems associated with V2G [38]. As with V2B, V2H co-optimization with rooftop solar or other smart appliances happens behind-the-meter and would not discharge to the grid, further eliminating expensive power electronic components and control systems which are required for reliability (i.e. anti-islanding protection) and the need for more precise measurement instrumentation (as required for net metering with rooftop solar or micro-wind). V2H, V2B, V2L and V2V topologies additionally benefit from reduced complexity as the need to coordinate and control tens to hundreds of individual users is eliminated, as in the case for V2G [20]. Utilizing EVs as emergency back-up generation has been shown to displace expensive diesel generators and to lower $C0_2$ emissions [41]. One caveat however is that V2B, V2H, V2L, and V2V topologies would all be considered energy products and their efficacy will largely be contingent on utilization frequency and duration as large energy throughput is known to be highly detrimental to battery lifetime as will be explained in Section 3.

1.2. Problem Statement

An important question is to what extent additional use of the vehicle battery will affect battery capacity over its lifetime. There have been several studies conducted towards this end, many of which claim these additional effects to be minimal or even negligible while others claim it to be a barrier to V2X [42–45]. Still others claim the additional battery degradation cost will be outweighed by the V2X income which would be generated [46]. While there is disagreement of the viability of V2X as a whole, there is a consensus that services which require a large energy throughput would likely be cost prohibitive as this would cause the greatest capacity degradation [42,45]. Due to this consensus, this review will focus more on V2G products as they constitute both a more lucrative market environment and less impactful operational profiles. However, as noted in Section 5.2, the various other V2X topologies can be economically feasible in certain cases.

To date there has been no published economic study to investigate battery degradation caused by real-world V2X service provision to a sufficiently sophisticated level which takes the interplay of Calendar and Cycling Aging effects and their fundamental drivers of Time, Temperature, State of Charge (SOC), Depth of Discharge (DoD), Charge Rate (C-rate), and Amp-hour (Ah) throughput into account. Truly empirical lifetime analyses would require time scopes of 10 years or more, which is both impractical and would be rendered obsolete at completion as battery technology is improving rapidly. Due to these challenges, semi-empirical electrochemical models have been developed which aim to model fundamental electrochemical phenomena mathematically while extracting rate relationships from what limited degradation data is available [47–55].

As the intention of this work is to review and explain the economic consequences due to battery asset degradation, semi-empirical electrochemical and combined electrochemical-thermal lifetime models are the focus of this work while other modeling methods such as equivalent circuit models, reduced order models, statistical methods, fuzzy logic, and other methodologies have been aptly covered in previous review articles and are mostly used to characterize battery operational behavior, not battery lifetime degradation [56–60]. Furthermore, this work does not attempt to incorporate all relevant electrochemical and particle physics theory, and rather focuses on the most important degradation mechanisms needed to predict battery life for economic analyses.

This review continues with an introduction to Battery Fundamentals in Part 2, followed by an explanation of Battery Degradation Mechanisms in Part 3. Part 4 is an overview of Battery Modeling Approaches and their limitations. The Economic Implications of battery degradation is then discussed in Part 5 followed by Conclusions in Part 6.

2. Battery Fundamentals

Lithium Ion batteries are complex electrochemical systems which

consist of four primary components: a negative electrode (anode), and positive electrode (cathode), an electrolyte, and a separator. Additionally, copper and aluminum current collectors are located at the positive and negative electrodes respectively. Degradation will occur at each element differently to contribute to overall life fade as explained in more detail in Section 3 on Battery Degradation Mechanisms.

2.1. Battery Cells

A battery cell consists of two electrodes (electronic conductors) which produce two half-reactions with the electrolyte (ionic conductor). Reductions occur at the positive electrode which is additionally referred to as the cathode while oxidations occur at the negative electrode which is additionally called the anode [61]. Individual battery cells are packaged together in a combination of string or series configurations to form battery packs which are controlled by a Battery Management System (BMS). The weakest cell in a string can affect the entire line output since the current which can be extracted from a cell within safe thermal operating conditions is a function of its internal resistance. Additionally, due to manufacturing deviations, weaker cells will charge and discharge more rapidly which can lead to overcharged cells and elevated temperature spots which can compromise the entire pack. Therefore it is crucial that the BMS monitors individual cells and balances the battery pack. Cell balancing refers to the practice of either removing excess charge of cells at risk of overcharge though heat dissipation in internal resistors or through moving charge from higher charged cells to lower charged cells such that all cells are maintained within a defined interval [62]. These two techniques are referred to as passive and active cell balancing respectively.

2.2. Anode

Anodes are typically graphite-based due to the low cost of material and the wide availability of carbon however graphite alone displays a high reactivity to electrolyte and therefore must be treated. Graphite anodes exhibit a moderate intrinsic specific capacity of 372 mA h g^{-1} however current commercial anodes will soon be unable to meet increasing energy density demands from electronic devices, electric vehicles, and energy storage applications [63]. Current graphite-based anode materials are effectively optimized and other anode materials such as metal oxides or alloying materials are either cost prohibitive or suffer reduced robustness. Therefore improvements in battery capacity and lifetime in commercial cells are through development of Silicon/Carbon (Si/C) composite anode materials or through the trend towards new, Nickel-rich cathode materials [14,64].

2.3. Cathode

Cathodes (positive electrode) consist of a complex lithiated compound material which will greatly affect the battery discharge profile, lifetime, and cost [65]. When speaking of Li-Ion battery chemistry, the cathode material is referenced as a graphitic anode is typically assumed. An overview of current commercial batteries, their chemical compounds, a snapshot of the technology characteristics, and current usages is presented in Table 1.

2.4. Electrolyte

The electrolyte must serve as an ionic conductor yet provide electronic insulation therefore it must exhibit a low viscosity and a high dielectric constant [66]. The reaction between the anode and electrolyte forms a passivating layer on the negative electrode (anode) surface known as the Solid Electrolyte Interface (SEI). Stability of the lithium battery depends on this reaction product. An SEI layer that is not passivating enough will continue to allow electrolyte molecules to reach the anode surface and will result in corrosion. An SEI layer that is too thick or insufficiently ionic-conductive can lead to unacceptably large increases in cell internal resistance, which is why only a few organic compounds can be used as solvents for the electrolyte [67]. Thus a key design goal of electrolytes and of film formation additives aims to result in a reaction product SEI layer that is ionically conducting, electronically insulating, and mechanically robust [68].

Traditionally Ethylene Carbonate (EC) has been used as electrolyte solvent and was previously thought to be indispensable; however, recent research has proven that EC free electrolyte battery cells perform better at higher voltages [8,69]. Ethel Methyl Carbonate (EMC) along with optimized amounts of “enablers”, additives which passivate the graphite electrode and thus enable an EC free cell to operate, has demonstrably improved performance [10].

Thus the electrolyte typically consists of an organic aqueous solvent (typically alkylcarbonates) with a salt compound (typically $LiBF_4$ or $LiPF_6$) which have become dominant in the market [68,70]. Although there is investigation into solid-state electrolytes and ionic liquid electrolytes, the organic aqueous solution is the primary technology used in commercial cells due to its superior ionic conductivity. Much research has been focused on improving the electrolyte performance and safety through either functional additives, enablers, or flame-resistant phosphate compounds and is seen as area which can still be improved in commercial cells [9,71].

2.5. Separator

The separator is a thin porous membrane which primarily serves to prevent the anode and cathode from physical contact while maintaining the free flow of ions [72]. For safety of the battery the separator must be able to shut the battery down when overheating occurs, as in the case of a short-circuit, to ensure thermal runaway is avoided [73]. Each battery chemistry has unique thermal runaway characteristics as can be seen in Fig. 2 with the worst to best ordering as LCO, NCA, NMC, LMO, and LFP.

3. Battery Degradation Mechanisms

3.1. General Terms

Battery State of Health (SOH) is negatively impacted through a reduction of total capacity and/or an increase in internal impedance. Typically definitions of SOH only focus on a measurement of capacity reduction (Capacity Fade) however internal impedance rise reduces the battery power delivery which is why increasing impedance is additionally referred to as Power Fade. Capacity Fade is caused by the irreversible Loss of Lithium Inventory (LLI) or through loss of active material (LAM), whereas internal impedance rise (Power Fade) is caused by increased kinetic resistance within system [75–77].

The SOH concept is important to define for when the battery asset reaches its End of Life (EoL). Currently there is no standard definition of EoL however many have taken the view that 20–30% reduction of capacity or a 100% increase from initial internal resistance constitutes EoL [78]. It is important to note that even at EoL, the battery is not fully depleted but still has a significant amount of capacity left (70–80%) which has lead several investigations into Battery Second Life (B2L) products as stationary storage systems or peak voltage provision in high power DC charging systems [79–81]. Furthermore, recent studies have suggested that batteries may continue to satisfy the majority of mobility needs down to 40% percent of remaining capacity [82]. Thus the need for a standardized definition of SOH and EoL along with accurate estimation and monitoring is clear.

3.2. Degradation mechanisms by cell component

Various degradation mechanisms act at each cell component to contribute to Capacity Fade and Power Fade, with the growth of the

Table 1
Current commercial batteries characteristics and usages.

	Manufacturer	Chemistry	Capacity	Configuration	Nominal Voltage	Weight	Volume	Energy Density	Specific Energy	Used in	
		Anode/Cathode	Ah		V	Kg	Liter	Wh liter^{-1}	Wh kg^{-1}	OEM	Model
1	AESC	G/LMO-LNO	32.5	Laminate	3.75	0.79	–	317	157	Nissan	Leaf
2	LG Chem	G/NMC-LMO	36	Pouch	3.75	0.86	0.49	275	157	Renault	Zoe
3	Li-Tec	G/NMC	52	Pouch	3.65	1.25	0.60	316	152	Daimler	Smart
4	Li Energy Japan	G/LMO-NMC	50	Prismatic	3.7	1.70	0.85	218	109	Mitsubishi	i-MiEV
5	Samsung	G/NMC-LMO	64	Prismatic	3.7	1.80	0.97	243	132	Fiat	500
6	Lishen Tainjin	G/LFP	16	Prismatic	2.3	0.52	0.23	200	89	Honda	Fit
7	Panasonic	G/NCA	3.1	Cylindrical	3.6	0.048	0.018	630	233	Tesla	Model S

Abbreviations used for Table 1 are: G = Graphite, LMO = Lithium Manganese Oxide, NCA = Nickel Cobalt Aluminum Oxide, NCM or NMC = Nickel Cobalt Manganese, LFP = Lithium Iron Phosphate, LCP = Lithium Cobalt Phosphate, LFSF = Lithium Iron Fluorosulfate, LTS = Lithium Titanium Sulfide, and LTO = Lithium Titanate Oxide (Titante is an anode material), LNO = Lithium Nickle Oxide.

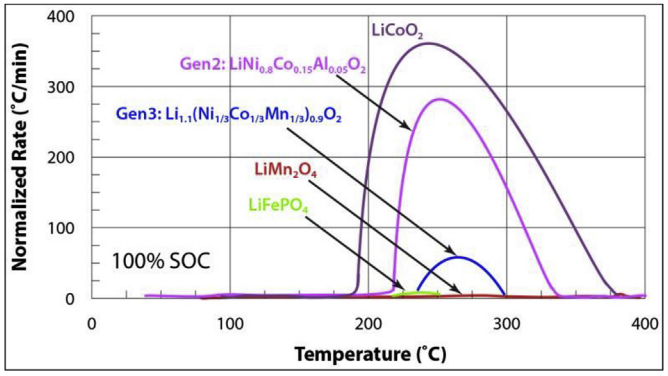

Fig. 2. Thermal Runaway Characteristics of NCA (purple), NMC (blue), LFP (green), and LMO (red) chemistries [74]. (For interpretation of the references to color in this figure legend, the reader is referred to the Web version of this article.)

Solid Electrolyte Interface (SEI), a passivation layer which forms on the anode, being the most prominent contributor. The SEI layer has been given extensive study due to its central importance not only in life degradation but in proper functioning of the battery. A stable and uniform SEI is required to protect against current collector corrosion at the anode from the highly reactive electrolyte, yet extensive or non-uniform SEI formation can result in dendrite growth, cracking, and a reduction in lithium access to the anode [52,71]. As an example, during the first full cycle up to 10% of the original battery capacity can be consumed in irreversible SEI formation though this amount has been reduced to 2–3% in recent cells [83]. Lithium plating, current collector corrosion, and mechanical failure are other prominent degradation mechanisms which are further explained in Part 3.3. Fig. 3 is a visual representation of the various aging mechanisms and where they take place.

3.3. Calendar vs Cycling Aging

These degradation mechanisms collectively result in two aging behaviors known as Calendar Aging and Cycling Aging which are

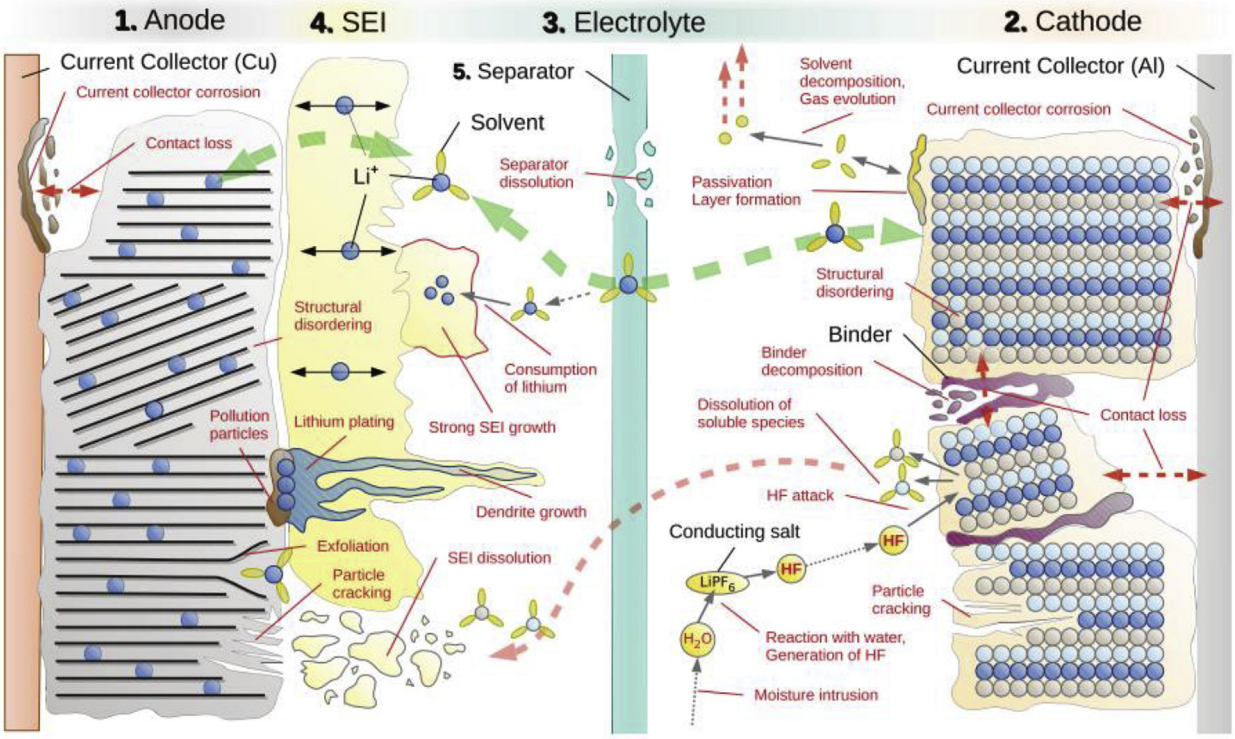

Fig. 3. Lithium ion battery aging mechanisms and battery cell structure [76].

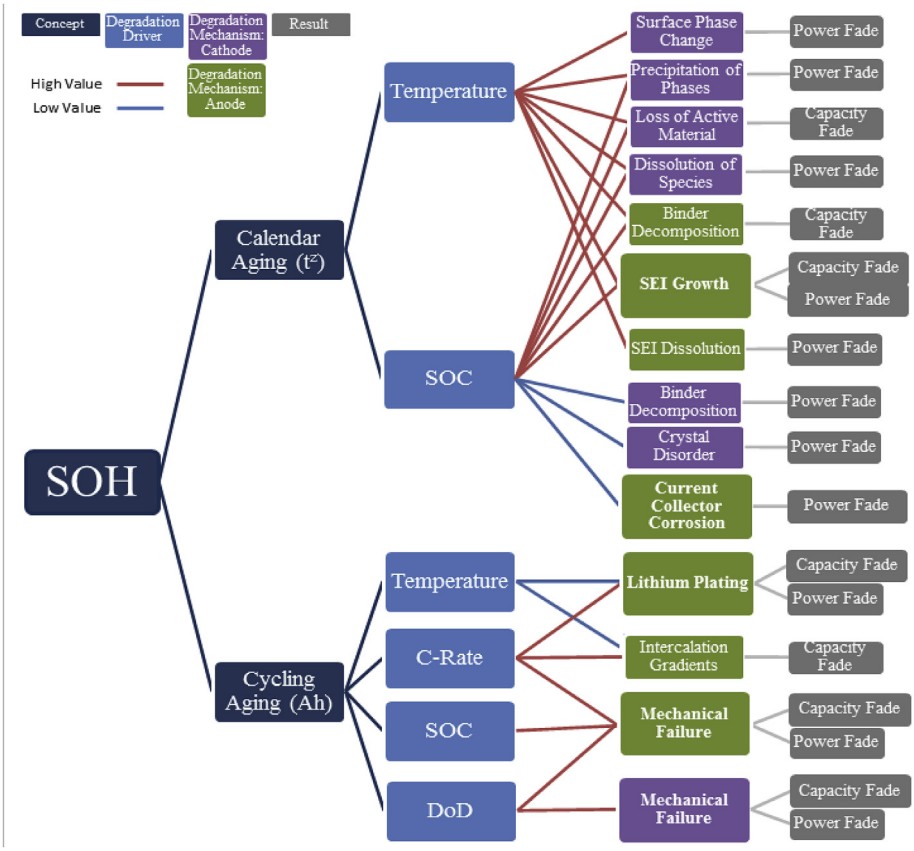

Fig. 4. Battery Degradation Flowchart. Shows conceptual and causal links between the Degradation Concepts (SOH, Calendar and Cycling Aging), Degradation Drivers (Temperature, SOC, C-rate, DoD), and various Degradation Mechanisms which could be controlled through active management of charging or V2X strategy.

exacerbated by degradation drivers (or stress factors). Calendar Aging is the degradation experienced when the battery is at rest and is dependent on Temperature and State-of-Charge (SOC). Temperature and SOC are coupled through an Arrhenius relationship which has been empirically proven to adequately model SEI layer growth and results in Calendar Aging having an underlying dependency on time (t^z) where z tends to be ½ [84–86]. Cycling Aging is the degradation resulting from battery usage and is dependent on the Temperature, SOC, charge current (C-rate), and Depth of Discharge (DoD or ΔSOC). C-rate is a representation of charge current normalized to battery capacity such that a current expressed as 1C would charge a given battery in 1 h. Similarly a current expressed as 2C would charge a battery in 30 min while a C/2 current would charge the battery in 2 h. While previously the underlying dependency of Cycling Aging was expressed as cycle number (N), recent research has shown that total Ah throughput, the total amount of energy extracted from the battery, is true underlying dependency of Cycling Aging [50,87,88].

Fig. 4 is a visual summary which shows conceptual and causal links between the Degradation Concepts (SOH, Calendar and Cycling Aging), Degradation Drivers (Temperature, SOC, C-rate, DoD), and various Degradation Mechanisms [75,76,85,89]. For example, the large size of the SEI Layer Growth box in Fig. 4 indicates that it is a prominent Degradation Mechanism while the green color of the box indicates that it acts at the anode. Fig. 4 also shows that SEI Growth is caused by high Temperatures and high SOCs while at rest (Calendar Aging), and results in a large amount of both Capacity Fade and Power Fade. Lithium Plating is another prominent Degradation Mechanism which acts at the anode, is caused by low Temperatures and high C-rates while cycling, and primarily results in a large amount of Capacity Fade with a lesser secondary result of Power Fade [68,75,76]. Mechanical Failure can occur at both the Anode and Cathode and is the result of volumetric changes during cycling which can lead to cracking of the SEI layer, lithium exfoliation, isolation of active electrode material, and contact loss at each current collector. Overcharge (Overpotential) and Overdischarge are also prominent degradation mechanisms which can cause gas evolution, particle cracking, and lithium plating [68,75,76]. Additionally, Current Collector Corrosion occurs at the anode and is caused by long periods of rest at low SOCs which results in a large contribution to Power Fade [75,76,85,89]. Apart from structural or manufacturing defects however, Overcharge and Overdischarge conditions will not be encountered in batteries which are properly protected by a BMS therefore are omitted here as V2X services will only operate batteries within manufacturer specified limitations. While Current Collector Corrosion can be avoided as well through manufacturer prescribed lower SOC limits, it is included in this visualization.

As previously mentioned, the total amp-hour (Ah) throughput refers to the total extracted energy of a battery throughout the course of its lifetime. Ah throughput is useful to compare the degradation effect of different usage profiles with various DoDs. Due to SOC effects, a cycle from SOC 100%- SOC 80% will not result in the same degradation as a cycle from SOC 40%- SOC 20% although they both would constitute a DoD of 20. By changing the X axis from cycle number to Ah throughput the true degradation effects of various cycle and usage profiles can be compared. Fig. 5 is a concise visualization of overall life Capacity Fade which differentiates the contribution of both Calendar and Cycling Aging effects.

While high temperatures trigger more Calendar Aging (chemical degradation) through increased SEI layer growth, low temperatures and high charge rates induce more Cycling Aging (mechanical degradation) through increased lithium plating. Additionally, high DoD cycling induces more mechanical failure especially if performed at high SOCs and high C-rates. To minimize Calendar Aging while the battery is at rest,

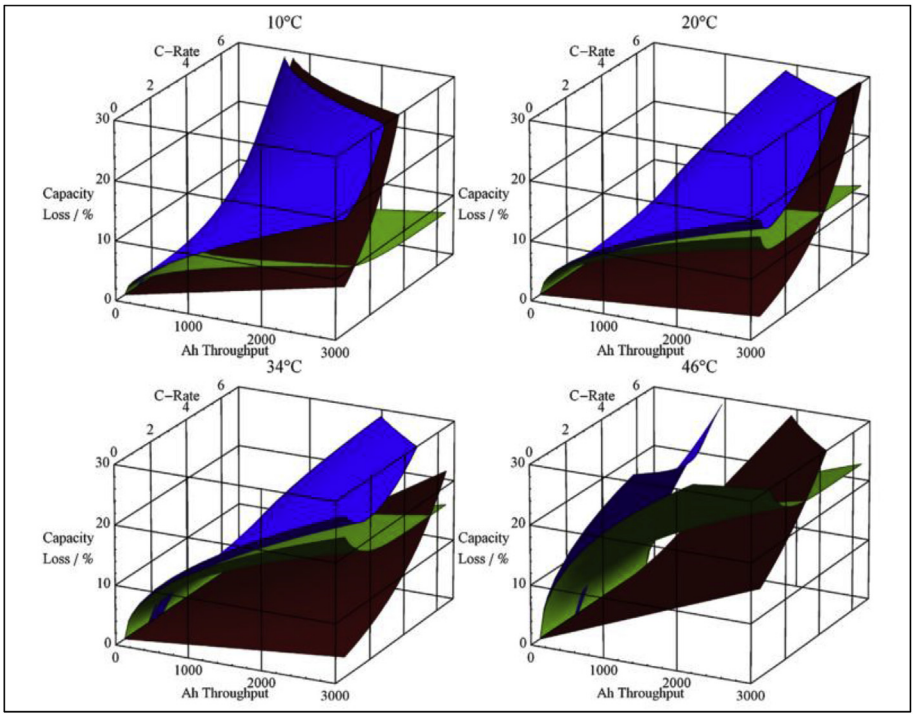

Fig. 5. Simulation of calendar life model and cycle life model for LMO-NMC chemistry as a function of discharge rate and Ah throughput for four experimental temperatures: 10, 20, 34, and 46 °C. (blue: total life loss; green: calendar life loss; and red: cycle life loss) [49]. (For interpretation of the references to color in this figure legend, the reader is referred to the Web version of this article.)

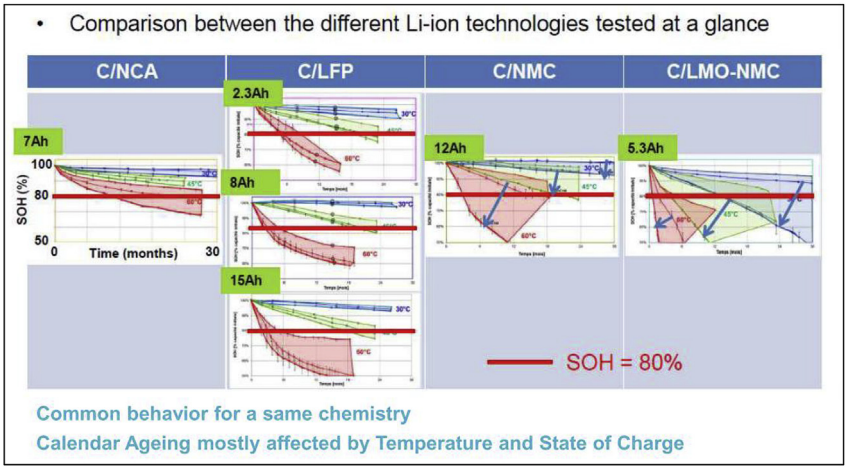

Fig. 6. Chemistry Effect on Calendar Aging for SOC = 30 (high), 65 (mid), 100 (low) and T = 30 °C (blue), 45 °C (green), and 60 °C (red) for various cell chemistries and battery manufacturers [54]. (For interpretation of the references to color in this figure legend, the reader is referred to the Web version of this article.)

maintain a low SOC and a low Temperature. To minimize Cycling Aging while the battery is in use, maintain a moderate Temperature, a low/moderate C-rate, and a low DoD centered around an optimal SOC point. Preliminary evidence suggests this optimal cycling point to be around SOC 50% as this is known to minimize joule heating yet more research is necessary [87,90].

As temperature is the most prominent environmental cause of battery degradation, proper thermal management is crucial and can even mitigate C-rate effects up to 2C [77]. Additionally cell temperature affects battery power output at extreme points such that high powered charging or discharging at very high or low temperatures would generate a diminished response. At all temperatures (except for very low, T < 10 °C) while operating in the pre-knee region, Calendar Aging is the dominant lifetime reducing factor. After the knee region, Cycling Aging becomes dominant due to a change in mechanism where capacity loss begins to be governed by graphite site loss (a mechanical process) rather than lithium loss (a chemical process) [91].

However an intelligent management strategy could prolong the knee region point until after the vehicle battery EoL. Understanding of fundamental battery degradation paired with the fact that most electric vehicles are immobile more than 90% of the time, implies that Calendar Aging is the dominant reduction factor for the majority if not all of lifetime. This is counter intuitive and leads to the conclusion that how a battery is managed while it is at rest will be the determining factor in lifetime performance.

3.4. Chemistry Dependency

When referring to Li-Ion battery chemistry, the cathode material is referenced as most commercial cells use a graphitic anode (Carbon). Due to long chemical names, batteries are referenced in short hand in the form of anode material/cathode material, however due the prevalence of Carbon (C) as an anode material, it is often omitted. An example battery cell with a Carbon anode/Nickle-Cobalt-Aluminum cathode would be written as C/NCA, or NCA. Along with NCA, the most common chemistries used in commercial cells are Iron Phosphate (LFP),

Nickle-Manganese-Cobalt (NMC), and Manganese Oxide/Nickle-Manganese-Cobalt blend (LMO-NMC). Consequently, each battery technology will exhibit varying sensitivities to degradation drivers due to differences in the cathode materials, electrolyte additives, and other nano-coatings.

Fig. 6, is a composite result of several Calendar Aging studies with various battery chemistry cells and manufacturers. A matrix of 9 storage conditions including 3 temperatures (30 °C, 45 °C, and 60 °C) and 3 SOC (30%, 65%, and 100%) were applied to all cells which were disconnected and kept in storage over a period of 2.5 years [92]. All cells of the same chemistry were from the same manufacturer with the exception of the Carbon anode/Iron Phosphate cathode batteries (C/LFP), which were compared across three different manufacturers. SOH was defined only in terms of Capacity Fade and the End of Life (EoL) criterion was defined as when cell capacity fell below 80% of original capacity.

The Blue, Green, and Red spreads provide a visualization of the aging effect of the storage Temperatures of 30 °C, 45 °C, and 60 °C, respectively. Within each spread, the effect of storage SOC can be seen as well, with the highest point in each temperature spread equal to SOC 30, the middle point = SOC 65 and the lowest point = SOC 100. Temperature sensitivity is manifested through the location and shape of each spread, while SOC sensitivity can be seen in the width of each spread. As can be seen in Fig. 6, there are pronounced differences in aging rates, aging profiles (how batteries lose capacity), and sensitivity to Temperature and SOC across battery chemistries.

However looking at Calendar Aging performance alone results in an incomplete picture; when referring again to Table 1 and Fig. 2, each chemistry has unique Cell Capacity vs Cell Potential ratios and safety characteristics. Thus choosing the “best” battery chemistry results in a tradeoff which will largely depend on the system application. A visual representation of this tradeoff for the current commercial battery technologies can be found in Figure S3 in the Supplementary Materials.

3.4.1. NCA

We can see from Fig. 6 that Nickle Cobalt Aluminum (NCA) is the superior technology in terms of Calendar Life as it exhibits the least sensitivity to both Temperature (seen in a close grouping of the Temperature spreads) and SOC (seen through the narrow width of each spread) and results in the least amount of Capacity Fade overall. Furthermore it can be concluded that for NCA the effect of Temperature is greater than the effect of SOC as there is no crossover between temperature spreads. Expressed differently, a higher storage temperature will always cause more capacity reduction than a lower temperature regardless of the storage SOC. To cause the least degradation, high temperatures should be avoided first with preference to lower SOCs as a low secondary importance. Additionally NCA exhibits the highest Specific Capacity vs Cell Potential ratio; however this all comes at the increased risk of thermal runaway and high cost. Consequently NCA requires the most investment to be operated safely in vehicles.

3.4.2. LFP

LFP generally exhibits a high Temperature sensitivity as seen in the large gaps between spreads but a low SOC sensitivity as seen in the narrow widths of the spreads. The effect of Temperature is again greater than the effect of SOC and a non-linear degradation rate (aging profile) is seen which is especially pronounced at high Temperatures. Interestingly, this study found that the same battery chemistry exhibited similar aging profiles regardless of the manufacturer, with the exception of the 15 A h manufacturer cell which is more prone to degradation at storage SOCs greater than 30%. To cause the least degradation, high temperatures should be avoided first with low SOC as a medium secondary importance. While the safety aspect is greatly improved as LFP is the least prone to thermal runaway, this comes at the cost of Specific Capacity vs Cell Potential and a reduced Specific Energy.

3.4.3. NMC

NMC exhibits a high Temperature sensitivity and a variable SOC sensitivity which is still greater than NCA or LFP at low temperatures and dramatically increases as temperature rises. Due to this variable SOC sensitivity, there is some crossover between Temperature spreads which results a more complex relationship. While Temperature is still the more dominant effect, due to increased SOC sensitivity low storage SOCs can compensate for the increased aging effect of higher temperature.

This can especially be seen when comparing the Red and Green crossover, it can be concluded that a cell stored at 60 °C and SOC 30 would result in less degradation than a cell stored at a lower storage temperature of 45 °C but at a higher SOC of 100. Similarly, from the Green/Blue crossover, a cell stored at 45 °C and SOC 30 would result in less degradation than a cell stored at 30 °C and SOC 100. To cause the least degradation, high Temperatures should be avoided and low SOCs preferred with increasing importance as temperature increases. NMC has the second highest Specific Capacity vs Cell Potential ratio and often overlaps NCA. The thermal runaway characteristics are also the second worst however are drastically reduced from NCA.

3.4.4. LMO-NMC

Meanwhile the Manganese Oxide + Nickle Manganese Cobalt (LMO-NMC) blend exhibits a very high sensitivity to both SOC and Temperature and the poorest Calendar Life performance resulting in the most Capacity Fade overall. Similarly to the pure NMC, there is significant crossover due to high SOC sensitivity which results in several scenarios where low SOC can compensate for higher temperature. Furthermore LMO-NMC exhibits an almost linear degradation (aging profile) across all storage conditions. To cause the least degradation, high temperatures and high SOCs should be avoided at all times. Pure LMO has the second best thermal runaway characteristics, therefore a blend with NMC is in attempts to improve safety (from LMO) while increasing Cell Potential vs Specific Capacity (from NMC).

4. Battery Modeling Approaches

This section consists of an overview of three semi-empirical lifetime models, so named due to their extrapolations of battery behavior based on experimental data, which have influenced many other models and research efforts. Each follows a similar process which consists of hypothesizing fundamental degradation equations, generating rate laws and other coefficients, and fitting the original hypothesis to experimental data to generate the general model. In all models the degradation effect from Calendar Aging and Cycling Aging is assumed to be additive. Further references to each will be known as the NREL model [50], the Wang Model [49], and the MOBICUS Model [55].

4.1. NREL Model

4.1.1. Model equations and approach

The NREL Model was originally based upon an NCA chemistry dataset presented in Refs. [7,93,94] which was later updated to incorporate an LFP chemistry [48,50,52,81,91,95,96]. The model assumes fundamental degradation behavior is similar for all lithium ion technologies but is tuned by degradation coefficients which are chemistry dependent. The primary model outputs are battery capacity (Q) and internal impedance (R) and both Calendar Aging and Cycling Aging are incorporated.

The equation for internal resistance is:

$$R = a_o + a_1 t^{1/2} + a_2 N \quad (1)$$

The equation for cell capacity is the minimum of the capacity loss attributed to the loss of active material lithium (Q_{li}) vs the loss of active sites (Q_{sites}) in the electrolyte of the cell:

$$Q = \min(Q_{li},\ Q_{sites}) \tag{2}$$

Where

$$Q_{Li} = b_o + b_1 t^z + \ldots \tag{3}$$

$$Q_{sites} = c_o + c_1 N + \ldots \tag{4}$$

The coefficients are rate constants for the time effect on Resistance (a_1), the cycle number effect on Resistance (a_2), the time effect on Lithium Loss (b_1), and the cycle number effect on Site Loss (c_1). The ellipses signify the fact that the final model is hypothesized and chosen from empirical fits based upon statistics, thus new terms could be introduced into the model equation depending on the aging data. Indeed [91] implied an existence of a cycle number dependency of lithium loss (Q_{li}) term to be denoted as b_2N, however this term does not exist in any know published representation of the NREL model and therefore has been omitted here. While z is understood to normally be ½ due to the well-known $t^{1/2}$ dependency of active lithium loss due to the SEI layer growth, the model nomenclature was generalized to allow for empirical fits which do not exhibit this dependency.

The model coefficients are developed from generalized rate constant equations which assumes an Arrhenius dependence on Temperature (θ_T), a Tafel dependence on Open Circuit Voltage (θ_{Voc}, which is related to SOC), and a Wöhler dependence on changes in Depth of Discharge ($\theta_{\Delta DOD}$).

$$\theta_T = exp\left[\frac{-E}{R_{ug}}\left(\frac{1}{T(t)} - \frac{1}{T_{ref}}\right)\right] \tag{5}$$

$$\theta_{Voc} = exp\left[\frac{\alpha F}{R_{ug}}\left(\frac{V_{oc}(t)}{T(t)} - \frac{V_{ref}}{T_{ref}}\right)\right] \tag{6}$$

$$\theta_{\Delta DoD} = \left(\frac{\Delta DoD}{\Delta DoD_{ref}}\right)^{\beta} \tag{7}$$

Furthermore the effect of all rate constant equations is assumed to be multiplicative.

$$\theta = \theta_{ref}\,\Pi\theta_k. \tag{8}$$

Note that E, α, β, and θ_{ref} are fitting parameters and is where the chemistry specific behavior is captured while R_{ug} is the universal gas constant and F is the Faraday constant. The reference parameters are chosen to normalize aging to standard conditions and are defined as follows: T_{ref} = 298.15 K, V_{ref} = 3.6 V, and ΔDOD_{ref} = 1. In short, the NREL model predicts incremental aging over an assumed standard aging profile [97]. This approach was chosen due to the reality that Calendar Aging (i.e. the effect of time) cannot be separated from Cycling Aging effects.

4.1.2. Knee region modeling

A discrepancy between model prediction and aging data was found in mid-to-high DoD cycling data, therefore later the c1 rate constant was updated to better account for the "knee region" where capacity loss is governed by the graphite site loss (mechanical process) rather than lithium loss (predominately chemical process) [91]. Calculations based on model extrapolation indicated that battery life would be over predicted by 25% if the knee region was not accounted for.

The hypothesized cause of the knee region was attributed to mechanical stress effects due to a combination of 1.) accelerated polymer failure at high temperatures, 2.) bulk intercalation strain, 3.) bulk thermal strain, and 4.) intercalation gradient strain accelerated by low temperature [91]. Therefore c1 was updated to account for these effects as follows[2]:

$$c_1 = c_{1,\,ref}\left\{exp\left(\frac{-E_a^{binder}}{R}\left(\frac{1}{T} - \frac{1}{T_{ref}}\right)\right)[m_1 DOD + m_2 \Delta T] + m_3\, exp\left(\frac{-E_a^{intercal}}{R}\left(\frac{1}{T} - \frac{1}{T_{ref}}\right)\right)\left(\frac{C_{rate}}{C_{rate,\ ref}}\right)\left(\sqrt{\frac{t_{pulse}}{t_{pulse,\ ref}}}\right)\right\}. \tag{9}$$

It was later shown that Bulk Intercalation Strains had the strongest correlation to capacity fade at the knee region. The updated model with the new c1 parameter was then applied to an LFP aging meta-dataset and was shown to be able to adequately predict 13 aging conditions with temperatures ranging from 0 to 60 °C [91].

4.2. Wang Model

The Wang model was based upon accelerated life testing of a large test matrix of battery conditions of the 1.5 A h 18650 LMO-NMC Sanyo technology which drew upon previous work which modeled cycle life of LFP cells [49,98]. This study also provided a thorough description of both the test conditions and the measurement techniques employed to characterize the batteries. Cells were characterized by four techniques: capacity characterization (with well-defined charge/discharge profiles), relaxation tests, Electrochemical Impedance Spectroscopy (EIS), and Hybrid Pulse Power Characterization (HPPC). Additionally, this study conducted a voltage differential analysis to examine the source of capacity loss and concluded that lithium (material) loss was the limiting factor thus the active site loss was not modeled.

The Calendar Life loss model was developed from fitting model parameters to a fundamental capacity loss equation which assumed an Arrhenius dependence on Temperature.

$$Q_{loss,\,\%} = A \cdot exp(-E_a/RT) t^{1/2} \tag{10}$$

Where A is the pre-exponential factor, E_a is the activation energy in J/mol, R is the gas constant, and T is the absolute temperature. As the test matrix did not include stored cells, the low rate (C/2) and shallow DoD (10%) cycling data set was taken as an approximate storage condition and the model parameters were fitted to result in the Calendar Life loss model. The result of the model fit is expressed in Equation (11).

$$Q_{loss,\,\%} = 14876 \cdot exp(-24.5kJ/RT) \cdot days^{1/2} \tag{11}$$

The degradation due to cycling was calculated by subtracting the Calendar Life loss model from the total loss measured from the data. The fundamental cycle loss equation was hypothesized from the rate effect of the C-rate and is of the functional form:

$$Q_{loss,\,\%} = B_1 \cdot exp(B_2 \cdot rate) \cdot Ah_{throughput} \tag{12}$$

Where B_1 is the pre-exponential fitting factor and B_2 an exponential fitting factor. Data from the 50% DoD cycling conditions were fitted to Equation (12) to result in the Cycle Life Model for the four temperature conditions with individual B_1 and B_2 factors per temperature as seen in Equation (13).

Cycle life model	
10 °C	$[0.0021exp(0.4278 \cdot rate)] \cdot Ah_{throughput}$
20 °C	$[0.0008exp(0.3903 \cdot rate)] \cdot Ah_{throughput}$
34 °C	$[0.0010exp(0.3107 \cdot rate)] \cdot Ah_{throughput}$
46 °C	$[0.0045exp(0.1826 \cdot rate)] \cdot Ah_{throughput}$

(13)

Finally a generalized equation to take all temperatures and rates into account was found by an empirical fitting of B_1 and B_2 factors of the cycle life loss model. Thus the overall Lifetime Model is represented by Equation (14).

$$Q_{loss,\,\%} = (aT^2 + bT + c)\exp[(dT + e) \cdot I_{rate}] \cdot Ah_{throughput} + f \cdot t^{\frac{1}{2}} \cdot \exp(-E_a/RT)$$

[2] Note in Ref. [91] the coefficient appears as c2 however there is no clear indication of why chronological order was not followed.

Coefficient values and units			
a	8.61E-6, 1/Ah-K^2	I_{rate}	C-rate
b	−5.13E-3, 1/Ah-K	t	Days
c	7.63E-1, 1/Ah	E_a	24.5, kJ mol^{-1}
d	−6.7E-3, 1/K-(C-rate)	R	8.314, J mol^{-1} K^{-1}
e	2.35, 1/(C-rate)	T	K
f	14,876, 1/day$^{1/2}$		(14)

It was shown that at lower temperatures (10 °C) life degradation exhibits a linear relationship as Cycling Aging is the dominant mechanism, while at high temperatures (46 °C) a more exponential relationship is seen due to Calendar Aging dominance. Understanding of the interrelation of C-rates, Temperatures, and Ah throughput lead to a concise visualization of Calendar vs Cycling Aging effects which was shown previously in Fig. 5.

4.3. MOBICUS Model

The MOBICUS Model is still in development and has been the product of ongoing research projects since 2007 [53–55,92,99,100]. Currently the **Mo**deling of **B**atteries **I**ncluding the coupling between **C**alendar and **Us**age aging (MOBICUS) project is expanding the model for more usage profiles and coupling the effects of previously developed aging models. The Cycling Aging model was the product of the SIMSTOCK project from 2007 to 2011 which investigated 3 Li-ion technologies while the Calendar Aging model was a product of the SIMCAL project from 2009 to 2012 which investigated 6 different Li-ion technologies. A summary of the technologies investigated in each project is presented in Table 2.

While databases of the aging characteristics of the previous battery chemistries were built throughout the SIMSTOCK and SIMCAL projects, only a few chemistries have been further developed into models which have been published in the literature. While the MOBICUS project seems to claim integration of all available chemistry datasets into the latest model iteration, it is not clear how each dataset is taken into account as there have been no comprehensive published articles to date. Thus the Calendar Aging and Cycling Aging model representations will be described in their limited capacities available in the literature along with the latest understanding of the final MOBICUS model.

4.3.1. SIMSTOCK Cycling Aging Model

The SIMSTOCK project representation of Cycling Aging is found in Ref. [55] for an LMO-NMC blend battery chemistry and was initially formulated as a polynomial expression of the form:

$$F(Y) = y_{00} + y_{01}\cdot X_1 + y_{02}\cdot X_2 + y_{03}\cdot X_3 + y_{04}\cdot X_4 \quad (15)$$

Where X_1 = current (A), X_2 = temperature (°C), X_3 = Ah throughput (A/s), and X_4 = ΔSOC (%) and the variable Y represented the total aging, considered as cumulative ampere-hours. The paper references the NREL model but notes that aging parameters are considered static throughout the life of the battery cell which is a limitation as the rates at which degradation parameters affect the overall life fade will change as the battery ages. Therefore to capture changes in degradation rate losses, the Cycling Aging model was adapted to calculate the differential capacity loss and was formulated as follows:

Table 2
SIMSTOCK and SIMCAL battery technologies.

	NCA	LMO-NMC	NMC	LFP
SIMSTOCK	Saft 7 A h	LG Chem 5.3 A h	–	LiFeBatt 8 A h
SIMCAL	Saft 7 A h	LG Chem 5.3 A h	Kokam 12 A h	LiFeBatt 8 A h LiFeBatt 15 A h A123 2.3 A h

$$\left(\frac{dQ_{Li}}{d(\sqrt{t})}\right) = a_j, \text{ where } \quad a_j = a_{00} + a_{01}\cdot X_1 + a_{02}\cdot X_2 + a_{03}\cdot X_4 + a_{04}\cdot X_4 \quad (16)$$

The model was then fitted to the results of the testing conditions which cycled the four parameters (X_1 - X_4) through all possible binary permutations (0,1) where 0 was the minimum condition and 1 was the maximum condition, resulting in eleven total tests. As this model is in derivative form it attempts to predict the instantaneous rate at which capacity declines during each battery test condition, then integrates each individual slope over time to result in the full capacity degradation. The paper derived three conclusions from the LMO-NMC Calendar Aging model: that the predominate aging effect was temperature, the effect of Ah throughput was greater than the effect of current, and that without stress, the coefficient a_0 is positive and indicated that the battery would regain capacity at low temperatures.

4.3.2. SIMCAL Calendar Aging Model

The SIMCAL Calendar Aging model is presented in Ref. [53] for an LFP battery chemistry which was subjected to six storage conditions for a total of 14 tests. Batteries were stored at SOC: 30, 65, and 100 while being subjected to temperatures of 30 °C, 45 °C, 60 °C, and a thermal cycling test which varied temperature from 30 to 45 °C. This model was also initially formulated as a derivative equation as follows:

$$\frac{dQ_{loss}}{dt} = k(T,\ SOC)\cdot\left(1 + \frac{Q_{loss}(t)}{C_{nom}}\right)^{-\alpha(T)} \quad (17)$$

Where:

- k (T, SOC) is the kinetic dependence of capacity fade evolution with Temperature (T) and SOC during storage.
- Q_{loss} (t)/C_{nom} is the fractional capacity loss at time *t*.
- (1 + Q_{loss} (*t*)/C_{nom})$^{-\alpha(T)}$ with α(T) > 0 is related to the diffusion limitation of solvent molecules inside the SEI layer which tends to decrease the capacity fade rate and is temperature dependent.

In order to express the total capacity loss as a function of time, the incremental representation seen in Equation (17) was integrated by setting α = 1 at t = 0 for Q_{loss} = 0 and resulted in:

$$Q_{loss}(t) + \frac{1}{2}\cdot\frac{Q_{loss}(t)^2}{C_{nom}} = k(T,\ SOC)\cdot t \quad (18)$$

Later it was noted that this representation did not fit the aging dataset well. Therefore the model was further generalized to allow for model tuning to aging data that did not follow an Arrhenius ($t^{1/2}$) evolution. This was accomplished by integrating Equation (18) and assuming that T and SOC remain constant to result in:

$$t = \frac{C_{nom}}{(\alpha+1)\cdot k(T,\ SOC)}\cdot\left\{\left(1 + \frac{Q_{loss}}{C_{nom}}\right)^{\alpha+1} - 1\right\} \quad (19)$$

Additionally the kinetic dependence of capacity fade (*k(T, SOC)*) was further expressed as follows:

$$k(T,\ SOC) = A(T)\cdot SOC + B(T) \quad (20)$$

$$A(T) = k_a\cdot\exp\left\{-\frac{Ea_A}{R}\cdot\left(\frac{1}{T} - \frac{1}{T_{ref}}\right)\right\} \quad (21)$$

$$B(T) = k_b\cdot\exp\left\{-\frac{Ea_B}{R}\cdot\left(\frac{1}{T} - \frac{1}{T_{ref}}\right)\right\} \quad (22)$$

Where R is the ideal gas constant (8.314 J mol K^{-1}), T is represented in Kelvin, SOC represented as a percentage, and T_{ref} was set at 298 K. The model parameters α and *k* were estimated through non-linear regression techniques to fit the baseline model to the aging data.

Storage temperature was shown to have a stronger effect on battery

life than storage SOC and that higher storage values of temperature and SOC impacted battery life more than lower values if the trend continues. The effect of temperature and SOC was most apparent in the 65 °C case which exhibited a $t^{1/2}$ dependency and a clear delineation of each SOC condition; however, at lower temperatures life fade exhibited a more linear degradation.

4.3.3. MOBICUS representation

What is known of the MOBICUS model representation can be found in Ref. [54] and seems to be an extension of the NREL representation. While NREL model Equations (1)–(4) are referenced, it seems that the most current version of Equation (3) was not incorporated and thus a $t^{1/2}$ dependency is assumed. The MOBICUS representation hypothesizes that since overall life degradation tends to be dominated by Calendar Aging effects, and that cycle frequency additionally influences the effect seen from those cycles, all degradation must therefore be time dependent. Thus, the MOBICUS model updates equations (1)–(4) for internal resistance R and battery capacity Q to become:

$$R = a_o + a_1 t^{1/2} + a_2 N \tag{23}$$

$$Q = \min(Q_{li}, Q_{sites}) \tag{24}$$

Where

$$Q_{Li} = b_o + b_1 t^{1/2} \tag{25}$$

$$Q_{sites} = c_o + c_1 t \tag{26}$$

It was claimed that with the MOBICUS representation, the knee region can be predicted with more accuracy, but it is unclear as to whether the updated NREL model parameter c_1 (active site loss model seen in Equation (9)) was taken into account. While the MOBICUS representation claims better fit to data so that Cycling Aging is not overestimated, there is no attempt to specify how this knee region develops or to what mechanism it is attributed to as in the NREL model. While may be possible to speculate the functional forms of the MOBICUS model from the SIMSTOCK and SIMCAL model outlines, there are no known published sources to confirm. Figure S4 and Figure S5 show the MOBICUS model compared to aging data and are included in the Supplementary Material as various battery chemistry aging profiles are compared at a glance.

4.4. Limitations of battery models

Semi-empirical battery models allow for extrapolation of future conditions which would be time and cost prohibitive to find empirically, however this entails they are inherently dependent on the aging data which is used to generate degradation rate laws. This limitation is manifested in several ways which are enumerated below.

4.4.1. Time resolution

The time resolution of the battery model is a limiting factor. As most models are based on average hourly values for temperature and minute values for SOC and other parameters, they cannot capture the effects of high frequency cycling or small deviations in Temperature. Additionally, effects of high charge rates other than average increases in temperature are not captured. This is important to note when attempting to evaluate degradation of fast grid services such as Frequency Regulation which operates at the seconds' time interval.

4.4.2. Data limitation

As noted in Ref. [97] current models do not capture effects of accelerating degradation mechanisms which could occur after 30% Capacity Fade. As rate relationships can only be assumed to hold true and are bounded by the underlying time period of the aging data, effects of degradation beyond 10 years cannot be predicted with certainty. Non-accelerated storage aging data is costly to generate due to the experimental and time requirements and it is unclear if low impact cycling could approximate storage conditions. The effects of extreme temperatures are not captured as none of the previous studies have investigated Temperatures above 50 °C and below 0 °C. From stress testing research it is clear though there would be pronounced degradation and potentially catastrophic cell failure at extreme temperatures. Finally, cell aging effects are known to be non-transferrable to the pack level as additional degradation beyond what could be explained by scaled effects exists [77]. This is likely due temperature non-uniformities within the battery pack which are not adequately captured by BMS temperature sensors, however it implies that scaled cell level characterized aging data may not adequately explain pack aging.

4.4.3. Cycling definition and frequency

The cycling frequency and cycling definition are known to drastically affect life degradation such that, any model which is based on accelerated cycling data alone could over predict battery life [52,93]. Various definitions of what constitutes a cycle exist depending on the application; such as when current passes through zero or another chosen point, the point where charge power slope changes, or the point where charge power returns to a previous value.

Currently there is no widely accepted standardization of test cycles; therefore it is crucial that battery cycles are well defined in aging studies. Cycle definitions should include charge rate, temperature (both ambient and effective cycle temperature), a well-documented charge profile, clear definition of what a cycle constitutes, and acknowledgement of rest times between cycles or between measurements. Clear definition of battery measurement and characterization techniques (EIS, charge/discharge, HPPC, etc.) should also be provided. Recent progress in battery test standardization been made in the US and China however more work is needed [101,102].

4.4.4. Chemistry specificity

Current models can only postulate degradation laws based on the chemistry of the underlying aging data. Each battery chemistry exhibits different sensitivities to degradation drivers, especially the effects of Temperature and SOC. Therefore it is important when employing semi-empirical models in economic cost evaluations to note the battery chemistry used and to understand that results are non-transferrable to other battery technologies. Furthermore some chemistries may be more prone than others to the Knee Region where capacity quickly drops due to increased mechanical degradation. This Knee Region is potentially avoidable or deferrable if battery usage conditions are constrained.

5. Economic Implications

As Calendar Aging tends to be the dominant aging factor, this implies that the Temperature and SOC at which a battery is at rest over time will have a more significant impact than any other consideration. This reduces down to the fact that battery degradation is time dependent. Additionally the total Ah throughput and how this current is extracted from the battery will further degrade SOH. Battery operational conditions will determine lifetime therefore all degradation drivers should be accounted for, however economic cost evaluations have only recently come to integrate sophisticated battery models. In the case of V2X services, the cost of the service provision should be outweighed by the revenue generated. While revenue calculation is relatively straightforward, without clear understanding of how a usage profile impacts battery life, battery degradation costs cannot be properly integrated to analyses.

5.1. First approximations of battery degradation costs

5.1.1. V2X cost fundamentals (Kempton and Tomic)

The first V2X cost evaluation can be found in the seminal works by Kempton and Tomic, which developed the fundamental equations of

battery asset costs for V2X [19,21]. While cost estimations for capital, purchased energy, and labor are well defined, battery degradation cost (c_d) is based on a Cycle Life only understanding of the battery which incorporates DoD but no other degradation drivers seen in Equation (27).

$$c_d = \frac{c_{bat}}{L_{ET}}, \quad L_{ET} = L_c E_s \, DoD \tag{27}$$

Where c_d is battery degradation cost, c_{bat} is the battery capital cost including labor for replacement of the battery, and L_{ET} is the lifetime energy throughput of the battery. L_c is the cycle lifetime number, E_s the total energy storage of the battery, and DoD is the depth-of-discharge at which L_c was determined. This formulization assumes that the extractable energy of the battery does not change over time for each cycle and that battery lifetime is defined as the number of cycles at a certain DoD.

5.1.2. Present Value of Throughput (PVT) (Neubauer et al.)

Net Present Value (NPV) is a widely accepted metric for economic valuation of assets which takes the Time Value of Money into account. Similarly, as Calendar Aging is the most important factor in battery asset fade, it follows that battery degradation costs must be also time dependent. A first attempt to include time into degradation costs is found in Ref. [80] which defined a Present Value of Throughput (PVT) metric to better account for the time dependency of battery energy as seen in Equation (28).

$$PVT = \sum_{i=1}^{n} \frac{(1 + 0.025)^{i-0.5}}{(1 + 0.10)^{i-0.5}} x_i \tag{28}$$

Where i = years, n = battery life in years, x_i = annual battery energy throughput in kWh. PVT accounts for the present value of both the capacity and cycle life of the battery assuming a discount rate associated with the time value of money of 10% per year and that the value of a kWh of energy storage increases at a rate of 2.5% per year [80]. While this formulation does include time, calculation of x_i would still require an understanding of both battery usage and degradation due to that usage. Furthermore the assumption that the value of battery energy increases over time may not always be accurate as that value is intrinsically a product of battery operation. Thus battery degradation costs are best informed by battery lifetime models which already incorporate all (or most) of the degradation drivers.

5.2. Battery degradation costs informed by battery models

5.2.1. Optimized charging algorithm (Hoke et al.)

The first known incorporation of a battery lifetime model to estimate degradation costs is found in Ref. [103] which develops an algorithm to optimize EV or PHEV charging based on both electricity and degradation costs. This work employs a simplified version of the NREL battery model to allow for reduced calculation time and is particularly interesting as it demonstrates an understanding for and incorporates nearly all degradation drivers for cost estimation. The results of the optimized charging power profile and strategy was dependent on the exogenous signal of electricity price with fixed inputs for ambient temperature (T), battery energy capacity (Q), initial SOC, plug-in time (t_0), and target time for full charge (t_{max}, where full charge was defined to be 90% SOC). Also note that only charge power was optimized where actual charge voltage and current was assumed to be controlled separately by the battery charger.

As seen in Fig. 7 a characteristic stepped power profile results as the optimal least cost charging strategy when given a constant electricity price and fixed inputs for ambient temperature (T = 25 °C), and thermal resistance (R_{th} = 0.002 °C W^{-1}). The tendency to charge later is due to Calendar Aging considerations which discourages spending time at high SOC. The spreading of charge over time, hence the stepped

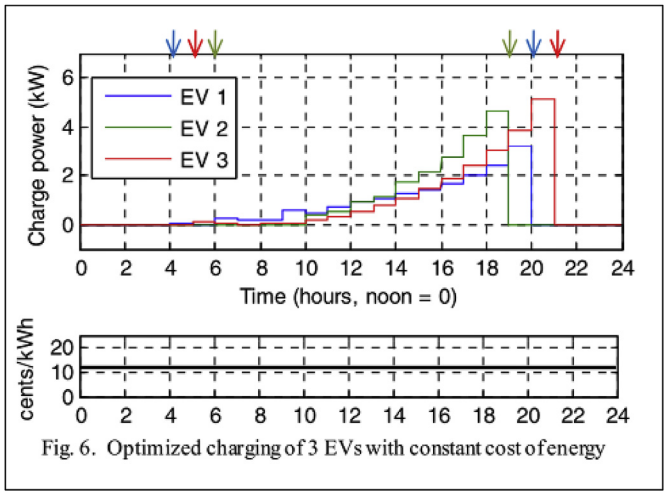

Fig. 6. Optimized charging of 3 EVs with constant cost of energy

Fig. 7. Optimized Charging Power Profile (upper panel) for three EVs at Fixed Electricity Price (lower panel). EV1 (blue) begins at SOC 35, EV2 (green) begins at SOC 30, and EV3 (red) begins at SOC 20 where the related colored arrows signify the user-specified plug-in and unplug time. Electricity price is constant at $0.12/kWh [103]. (For interpretation of the references to color in this figure legend, the reader is referred to the Web version of this article.)

power profile, is due Cycling Aging considerations which discourages high power (high current) charging to minimize temperature rise.

Later the effect of a variable electricity price and V2G power exportation was explored in vehicles with good thermal control (R_{th} = 0.0004 °C W^{-1}). In this example vehicles exported power immediately to lower resting SOCs even if this required a higher powered step charge later, again leading to the conclusion that minimization of Calendar Aging effects outweigh subsequent increases in Cycling Aging effects. In all instances the optimized charge profile was found to outperform other charge strategies and resulted in prolonging battery life between 4% and 50% over other strategies. This leads to the conclusion that if temperature can be adequately controlled, bulk power V2G exportation can be beneficial to minimize battery degradation costs even before including the primary additional value of revenue generation.

5.2.2. V2X service cost study (Wang et al.)

While previously shown that bulk energy transfer can be beneficial in certain circumstances, typically extended periods in this operational mode is highly detrimental [21,42]. Therefore grid services which require extended bulk energy transfer constitute the highest cost V2G service however several other services exist. In Ref. [104] the previously explained Wang battery model was paired with a lumped thermal model from Ref. [105] and the V2G-SIM software platform [82,106] to quantify battery degradation costs associated with driving only vs driving paired with a range of V2G services. The degradation effects of providing Peak Load Shaving, Frequency Regulation, and Net Load Shaping services were quantified by assuming each vehicle repeated the same itinerary for 10 years which consisted of daily driving and service provision profiles. Only capacity reduction was studied as internal impedance rise was omitted. All battery degradation costs were calculated assuming a replacement battery cost of $6000.00 and an EoL of 30% reduction of initial capacity.

5.2.2.1. Peak Load Shaving. When Peak Load Shaving was assumed to be provided every day for 10 years, the resultant additional capacity reduction ranged from 2.79%–9.69% over the 31.41% reduction from the base/uncontrolled charging scenario, highlighting the detrimental effect of extensive bulk power transfer. However based on [107] providing Peak Load Shaving every day is unrealistic and is likely only to be called during times of emergency, approximately 20 times per year. Therefore V2G emergency Peak Load Shaving was calculated

for the 20 hottest days of the year and was found to increase capacity losses by 0.38% with an L1 charger and 0.82% with an L2 charger over the base/uncontrolled charging case. The battery degradation cost from the 2-h emergency Peak Load Shaving (V2G) grid service was calculated to be $0.38 using an L1 charger at home and $0.82 using an L2 charger at home.

5.2.2.2. Frequency regulation. It was assumed that vehicles could adequately follow a Frequency Regulation signal from 19:00–21:00 every day based on results from Ref. [31]. The regulation signal was based on the PJM market RegD signal which is a fast-response signal designed to have zero net energy over each 15 min contract period. The Frequency Regulation service resulted in an average additional 3.62% capacity loss with an L1 charger and an additional 11.15% loss with L2 charging over the base case. The battery degradation cost from the 2-h Frequency Regulation was $0.20 using L1 charging and $0.46 using L2 charging.

5.2.2.3. Net Load Shaping. Net Load Shaping consists of flattening the shape of the system load profile i.e. filling in valleys while reducing the peak. While V1G (smart charging/unidirectional) was found to help reduce the system peak, V2G could both flatten the peak and shift consumption to off peak hours. The increased load shifting potential of V2G does come at an increased cost however as it would require deeper cycles and more bulk energy transfer than V1G. Therefore V2G Net Load Shaping service resulted in an additional 1.18% capacity loss with L1 charging and 2.60% with L2 charging over the base case. The battery degradation cost from the load shaping service was calculated for 20 days per year as $1.18 using L1 charging and $2.60 using L2 charging at home.

Overall it was concluded that V2G services could be dispatched in ways that result in very little additional cost to EV owners but extended bulk energy transfer services would likely be cost prohibitive.

5.2.3. V2G battery chemistry impact study (Petit et al.)

In Ref. [108] a semi-empirical model which incorporated both Calendar and Cycling Aging was used to assess the impact of V2G and the charging strategy on battery lifetime. This model attempted to capture chemistry effects as well and was verified using the same aging data used in Ref. [51] for an A123s 2.3 A h LFP cell and from the MOBICUS project for a Saft VLGP 7 A h NCA cell. The model assumed Calendar Aging was dominated by Temperature and SOC while the Cycling Aging was dominated by Temperature and C-rate (current) thus the other degradation mechanisms were omitted. One model simplification was that one form of aging could take place at a time, assuming that Calendar Aging was already taken into account when Cycling Aging occurred. The battery life effect of different charging strategies characterized through cycling profiles referred to as: Just In Time, Charge When You Can, Strong V2G, and Light V2G, which were compared to the Nominal Strategy of charging upon plug-in.

5.2.3.1. Results. The Nominal case consisted of medium DoD cycling with a relatively high average SOC and long periods of rest at high SOC. The Just In Time strategy consisted of medium DoD cycling with low average SOC and long periods of rest at low SOC. The Charge When You Can strategy consisted of very low DoD cycling, a high average SOC over time, and long periods at high SOC. The Strong V2G scenario consisted of several high DoD cycles, a medium average SOC, and long periods at low SOC. Finally the Light V2G consisted of high DoD cycling, a medium average SOC, and long periods at low SOC. These trends are summarized in Table 3.

The capacity loss results of each charging strategy are summarized Fig. 8 for both chemistries. The most notable result is how different the two technologies are affected by the charging strategy and that NCA exhibits superior capacity retention over LFP for every strategy. Overall the Just In Time strategy is the best as it simultaneously mitigates Calendar Aging by having long periods of storage at low SOC and does not require large DoD cycling which mitigates Cycling Aging compared to the other strategies. For LFP the Just In Time strategy results in a 3.5% capacity reduction compared the Nominal of 5.6% while for NCA the strategy benefit is less significant with 2.2% capacity reduction compared with the Nominal of 2.3%.

Table 3
General characteristics of various charging strategies.

	DoD Cycling	Average SOC	Rest SOC
Nominal	Mid	High	High
Just in time	Mid	Low	Low
Charge when you can	Low	High	High
Strong V2G	High (×3)	Mid	Low
Light V2G	High	Mid	Low

When looking closer at LFP, the Just In Time and Light V2G strategies cause the least degradation and actually decrease the life loss when compared to the Nominal case. However the Strong V2G case, which would require large amounts of battery throughput, is only slightly worse than the Nominal strategy. These two observations lend to the conclusion that incorporation of some level of V2G can be beneficial to battery life regardless, but that significant levels of V2G usage should be evaluated against the revenue benefit. For LFP the additional life loss of the Strong V2G strategy is only 0.02% over the Nominal and would likely be outweighed by revenue.

When looking at NCA the situation changes however as the Charge When You Can strategy exhibits less life loss than the Light V2G. Referring again to Fig. 6 however this does not seem surprising as the NCA Calendar Aging effect has a low sensitivity to SOC, therefore periods stored at high SOC would only have a slightly more negative impact compared with storage at low SOC on life fade. However for NCA the Strong V2G (4%) is worse than the Nominal (2.6%) and all others. This result would imply that the Calendar Aging mitigating effect of a low storage SOC is outweighed by the large DoD and subsequent increased Cycling Aging. This is an interesting result as it conflicts with [103] which also based on an NCA chemistry and concluded that the DoD effect on capacity loss was very small compared to the Temperature and SOC effects. One possible explanation is that the three large DoD swings raises the average battery temperature much higher than normal which would induce more capacity degradation. Why this effect would be more prominent for NCA and not seen in the LFP results is not clear however as LFP is known to be more Temperature sensitive.

While the Just In Time strategy resulted in the least Capacity Fade there was little difference compared to the Light V2G scenario in both chemistries. This study indicates that certain chemistries are better suited to certain usage profiles; therefore the cost effectiveness of V2X products may be chemistry dependent. This hypothesis may be evidenced by the different chemistry employed by Tesla for their vehicle (NCA) vs storage batteries (NCM).

5.2.4. V2X as prolonging life (Uddin et al.)

The first known paper to outright claim the positive life effect of V2X services can be found in Ref. [87]. While here an Equivalent Circuit Model (ECM) was employed, it was fitted with battery aging data effectively making it a semi-empirical ECM as each parameter varies over time and in response to degradation drivers. Capacity Fade and Power Fade were both investigated and SOH was defined such that EoL would be encountered if either end condition was met for Capacity Fade (80% remaining initial capacity) or Power Fade (100% increase in initial internal resistance). The model was populated with a robust aging dataset of 3 A h NCA 18650 cylindrical cells from an unnamed manufacturer. Fifty long-term aging tests with a well-defined experimental protocol were conducted under a wide range of operational conditions spanning $0\,^{\circ}C < T < 45\,^{\circ}C$, $15\% < SOC < 95\%$, $0\% < DoD < 80\%$.

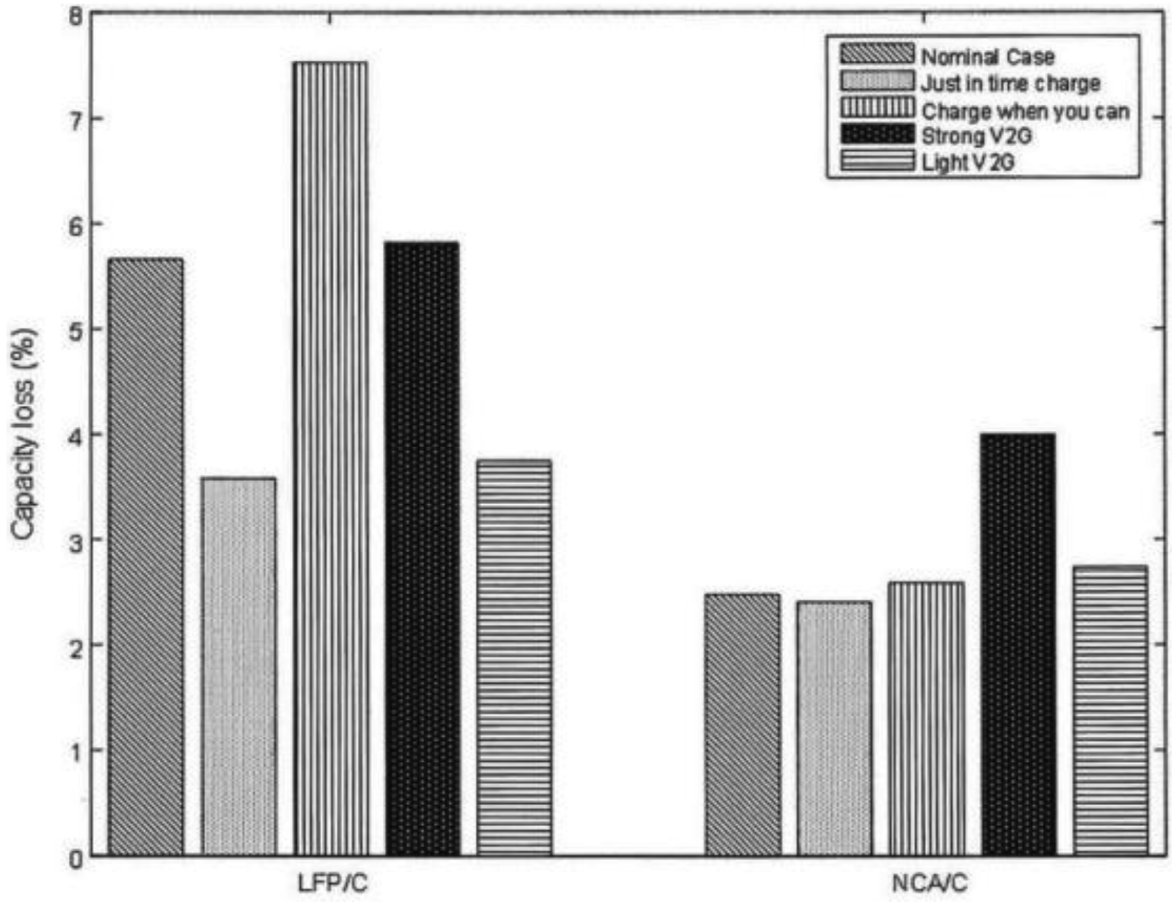

Fig. 8. Comparison of Capacity Loss due to various charging and V2G profiles for LFP and NCA Battery Chemistries [108].

Additionally each test condition was conducted on three separate cells to ensure robustness. Instead of using a phenomenological model, this work opted to instead fit a generalized model without hypothesizing rate constants with a fractional polynomial of the form:

$$Y = Y_0 + \alpha X^{\beta} \tag{29}$$

Where Y was either Capacity or Resistance, Y_0 was the corresponding value determined from the initial characterization test, X was either time or Ah throughput (K) and α and β were fitting parameters found through linear interpolation.

5.2.4.1. Vehicle–to-Building (V2B) optimization. In contrast to previous studies, this work proposed a V2B topology where EVs would discharge into a larger BESS, pumped storage, or compressed air system intermediary which could be used for either energy arbitrage or for flattening/shifting peak consumption of the commercial building to off-peak hours. V2B discharge was managed with the primary goal to minimize battery degradation through an iterative algorithm which compared the expected degradation cost at an initial resting SOC_i to the expected degradation cost of a lower SOC_{i+1} (Calendar Aging Mitigation) where ΔSOC was discharged to the storage intermediary. If SOC_{i+1} was found to be beneficial, the algorithm next compared whether the life gains from resting at SOC_{i+1} would outweigh the Cycling Aging induced to discharge ΔSOC and if all conditions were true, the algorithm would discharge to SOC_{i+1} , update it as the new SOC_i , and continue in increments of 1% ΔSOC until the optimal resting SOC was reached.

5.2.4.2. Results. This study only used V2B to minimize battery degradation cost and did not optimize financial gains vs battery degradation cost. While this V2B topology would result in a bulk energy transfer product, results indicated that both Capacity Fade and Power Fade could be reduced in certain circumstances. If a vehicle arrived with an initial SOC between 79 and 62%, discharging an additional 8–40% through V2B could reduce Capacity Fade by 6% and Power Fade by 3% over the first three months. While the V2B optimized algorithm was employed with an opportunistic charge strategy (analogous to Charge When You Can in Ref. [108]), the authors noted that incorporating a Just-in-Time strategy would likely deliver more pronounced life gains.

Next the V2B algorithm was investigated in a case study which tracked actual driving patterns of 349 EV, PHEV, and Fuel Cell EV (FCEV) owners and calculated the available V2B energy when integrated with an actual energy usage profile of commercial building. It was found that vehicles could provide 2.8 MW h of energy weekly which would equate to a 0.145 GW h annual energy arbitrage potential. Additionally, Capacity Fade was reduced up to 9.1% and PF by up to 12.1% for vehicle owners which translated to an annual savings of $555.00 for a single EV owner when assuming a replacement battery cost at $200/kWh.

6. Conclusions

6.1. Battery Degradation

Li-ion batteries are complicated electrochemical systems with non-linear interdependencies which exhibit two complementary aging behaviors known as Calendar Aging and Cycling Aging. Calendar Aging is dependent on the degradation drivers of Temperature and SOC which are coupled through an Arrhenius relationship which results in an

underlying dependency on time (t^z) where z tends to be ½. Cycling Aging is the degradation resulting from battery usage and is dependent on the drivers of Temperature, SOC, charge current (C-rate), and Depth of Discharge (DoD or ΔSOC). Cycling Aging results in an underlying dependency on total extracted energy (Ah throughput) rather than cycle number (N) as previously thought. Furthermore, each battery chemistry will exhibit varying sensitivities to these degradation drivers thus it is imperative that aging data is characterized by its underlying chemistry. Each of these degradation drivers influences fundamental mechanical and chemical degradation mechanisms to impact battery State of Health (SOH). SOH is reduced through either a decrease in total battery capacity (Capacity Fade) or an increase in internal impedance (Power Fade).

Capacity Fade is caused by the irreversible loss of active lithium material while internal impedance rise (Power Fade) is associated with increased kinetic resistance within the system, both of which are mostly attributed to an increased Solid Electrolyte Interface (SEI) layer growth. While high temperatures trigger more Calendar Aging (chemical degradation), low temperatures and high C-rates induce more Cycling Aging (mechanical degradation). To minimize Calendar Aging while the battery is at rest, maintain a low SOC and a low Temperature. To minimize Cycling Aging while the battery is in use, maintain a moderate Temperature, a low/moderate C-rate, and a low DoD centered around an optimal SOC point, which may be around SOC 50% as this point is known to produce the least joule heating, however more research into this phenomena is warranted.

At all temperatures (except for very low, $T < 10C$) while operating in the pre-knee region, Calendar Aging is the dominant lifetime reducing factor. After the knee region, Cycling Aging becomes dominant due to a change in mechanism where capacity loss begins to be governed by graphite site loss (a mechanical process) rather than active lithium loss (predominately chemical process). However an intelligent battery management strategy could prolong the knee region point until after the vehicle EoL. This understanding paired with the fact that most vehicles are immobile more than 90% of the time [109,110], implies that Calendar Aging is the dominant reduction factor therefore the battery management strategy while at rest will bound lifetime.

6.2. Battery Lifetime Models

Truly empirical battery lifetime analyses would require time scopes of 10 years or more, which is both impractical and would be rendered obsolete at completion as battery technology is improving rapidly. Due to these challenges, semi-empirical lifetime models have been developed which aim to represent fundamental electrochemical phenomena mathematically while extracting rate relationships from what limited degradation data is available. Semi-empirical models are preferred over other methods for economic analyses as they allow for extrapolation beyond experimental aging conditions while being based on electrochemical phenomena. The three primary semi-empirical models explored in this review are known as the NREL Model [97], the Wang Model [49], and the MOBICUS Model [54,88] which have influenced or have been incorporated into several other models and research efforts. A summary of the degradation drivers of Calendar and Cycling Aging, the dependencies each model accounts for, and the relationship between models is found in Table 4.

While the NREL Model seems to be the most well developed, it is limited to two chemistries and is based on population data primarily from geosynchronous orbit satellite life qualification tests. The Wang Model is also well developed with additional insights related to which degradation mechanisms bound capacity loss and the visualization of the Calendar vs Cycling Aging effects as seen in Fig. 5. However the Wang Model is limited to the NMC-LMO chemistry and does not employ actual storage data as it assumed low C-rate, low DoD rate cycling data would be comparable. The MOBICUS project has access to the most robust aging data set from the greatest variety of battery chemistries; however the overall modeling approach to couple Calendar and Cycling Aging is not clear as there are no known published works. Therefore model dependencies must be inferred from previous models developed out of the research of the SIMSTOCK and SIMCAL projects.

While semi-empirical battery models are the best tools for predictive analyses due to the cost prohibitive elements of empirical full life-cycle testing, they are inherently limited by their source data. This limitation is manifested in several ways:

1.) Time resolution: current models do not take micro cycling into account and calculate temperature degradation from average impact normally at an hourly timeframe. Therefore they cannot be used to estimate Frequency Regulation or other high frequency charge/discharge service costs.
2.) Data Limitation: It is difficult to predict beyond 10 years and below 30% Capacity Fade as no empirical dataset has been generated, lack of data at extreme temperatures. Additionally cell-to-pack translations of aging data are known to produce biased results. This is due cell-to-cell variations within the battery pack which produce temperature non-uniformities and thus non-uniform aging.
3.) Lack of test cycle standardization: cycle definitions should include charge rate, temperature (both ambient and effective cycle temperature), a well-documented charge profile, clear definition of what a cycle constitutes, and acknowledgement of rest times between cycles or between measurements. Clear definition of battery measurement and characterization techniques (EIS, charge/discharge, HPPC, etc.) should also be provided.
4.) Chemistry limitation: different Li-ion chemistries have drastically different aging profiles, thus the need to expand current models to additional chemistries is clear.

Therefore economic analyses of battery assets should contain sufficient electrochemical detail to account for chemistry specific degradation behavior to produce results based on physical reality.

6.3. Economic Implications of Battery Degradation

Calendar Aging tends to be the dominating life effect in vehicular applications, this reduces to Time being the most important component of degradation; thus battery degradation cost calculations should be time dependent. Battery Temperature is also highly impactful followed by SOC and the total Ah throughput, however economic cost calculations to date have mostly focused on cycle number as the determining factor of lifetime.

For Cycling Aging there is consensus that the amount of energy which is extracted (Ah throughput) from the battery will be more significant than number of cycles however, the manner of how the energy is extracted (i.e. at what temperature and what C-rate) will still be important. Charging strategies for vehicular applications should therefore be first designed to mitigate Calendar Aging, but ideally should be able to balance both Calendar and Cycling Aging effects.

The best battery management strategy should be based on three principles with decreasing order or importance: 1.) Minimize Temperature rise, 2.) Minimize time spent at high SOC, and 3.) Minimize average charge power (C-rate). Therefore relatively simple designs such as delayed or “Just-In-Time” charge strategies will always outperform the typical charge when plug-in, regardless of battery chemistry. Furthermore, V2X services may in fact prolong battery life rather than shorten it by contributing to the three principles if incorporated with sufficiently sophisticated battery models. Even bulk energy transfer V2X products with their high Ah throughput, can be beneficial when incorporated with a holistic battery management strategy. Furthermore, the value of V2X products may in fact be chemistry dependent as some chemistries are more suited than others to specific usage profiles. While there still have been no sophisticated studies to look at the degradation effects of fast charging and

Table 4
Summary of semi-empirical battery degradation model dependencies.

		Calendar Aging			Cycling Aging				Chemistry			
		Temp	SOC	Time	Temp	SOC	C-rate	DoD	NCA	LFP	NMC-LMO	NMC
NREL		✓	✓	✓	✓	✓	✓	✓	✓	✓		
	[103]	✓	✓	✓	✓	✓	✓	✓	✓			
	[111]	✓	✓	✓	✓	✓	✓	✓	✓			
Wang		✓		✓	✓		✓	50%			✓	
	[51]				✓		✓	✓		✓		
	[104]	✓		✓	✓		✓	50%			✓	
MOBICUS		✓	✓	✓	✓	Unclear	✓	✓	✓	✓	✓	✓
	[92]	✓	✓	✓						✓		
	[55]				✓	✓	✓	✓			✓	
	[108]	✓	✓	✓	✓		✓		✓	✓		

discharging as would be employed in a Frequency Regulation product, the final and key conclusion is that integration of V2X services with controlled charging regimes could in fact prolong battery life while delivering tangible energy and cost savings to both EV owners and building managers.

We envision that V2X services could be cost-effectively incorporated with vehicle battery management strategies using the following principles.

V2X Frequency Regulation:

- Upon plugin for long period, decrease SOC to lowest level such that the charging rate required to reach the SOC needed for the next trip would not significantly increase battery temperature.
- Perform Frequency Regulation around this nominal SOC value (if temperature rise can be sufficiently contained).
- Step charge back up to required SOC level for mobility needs at last possible moment.
  - o Timing for this step charge should calculate trade-off between market participation duration and battery temperature rise due to increased charge rate.

V2X Energy Arbitrage or V2B:

- Upon plugin for long period, decrease SOC to lowest level such that the charging rate required to reach the SOC needed for the next trip would not significantly increase battery temperature while using discharge for bulk power V2X service simultaneously.
- Sit until last possible moment
- Step charge back up to required SOC for mobility needs at last possible moment.

Without V2X:

•Upon plugin for long period, decrease SOC to lowest level such that the charging rate required to reach the SOC needed for the next trip would not significantly increase battery temperature.
•Sit until last possible moment
•Step charge back up to required SOC level for mobility needs at last possible moment.

Acknowledgements

This work was financially supported by the Insitut VEDECOM, a French Public-Private research institute and one of the Institutes for the Energy Transition *(Instituts pour la transition énergétique, ITE)* under the Shared Mobility and Energy research domain, Project ID MOB.06. The author claims no conflict of interest. This work benefitted from the feedback of the various journal reviewers and conference attendees. In addition, this work was greatly improved due to the input of Yannick Perez from the University of Paris SUD, François Colet from the Institut VEDECOM, and Doug Black from Lawrence Berkeley National Laboratory.

Appendix A. Supplementary data

Supplementary data related to this article can be found at http://dx.doi.org/10.1016/j.jpowsour.2018.06.053.

References

[1] International Energy Agency, Global EV Outlook, Beyond One Million Electric Cars, 2016, (2016) doi:EIA-0383(2016).
[2] International Energy Agency, Global EV Outlook, Two Million and Counting, 2017, (2017), http://dx.doi.org/10.1787/9789264278882-en.
[3] UNFCCC Conference of the Parties, Adoption of the Paris Agreement, The United Nations, Paris, 2015 doi:FCCC/CP/2015/L.9/Rev.1.
[4] International Energy Agency, Transport energy and CO2: moving towards sustainability, International Energy Agency (IEA), Paris (2009), http://dx.doi.org/10.1787/9789264073173-en.
[5] Bloomberg New Energy Finance (BNEF), Here's how electric cars will cause the next oil crisis, BNEF (2016), https://www.bloomberg.com/features/2016-ev-oil-crisis/ , Accessed date: 21 March 2018.
[6] K. Abe, H. Yoshitake, T. Kitakura, T. Hattori, H. Wang, M. Yoshio, Additives-containing functional electrolytes for suppressing electrolyte decomposition in lithium-ion batteries, Electrochim. Acta 49 (2004) 4613–4622, http://dx.doi.org/10.1016/j.electacta.2004.05.016.
[7] M. Broussely, P. Biensan, F. Bonhomme, P. Blanchard, S. Herreyre, K. Nechev, R.J. Staniewicz, Main aging mechanisms in Li ion batteries, J. Power Sources 146 (2005) 90–96, http://dx.doi.org/10.1016/j.jpowsour.2005.03.172.
[8] R. Petibon, L. Rotermund, K.J. Nelson, A.S. Gozdz, J. Xia, J.R. Dahn, Study of electrolyte components in Li ion cells using liquid-liquid extraction and gas chromatography coupled with mass spectrometry, J. Electrochem. Soc. 161 (2014) A1167–A1172, http://dx.doi.org/10.1149/2.117406jes.
[9] J.C. Burns, A. Kassam, N.N. Sinha, L.E. Downie, L. Solnickova, B.M. Way, J.R. Dahn, Predicting and extending the lifetime of Li-Ion batteries, J. Electrochem. Soc. 160 (2013) A1451–A1456, http://dx.doi.org/10.1149/2.060309jes.
[10] L. Ma, S.L. Glazier, R. Petibon, J. Xia, J.M. Peters, Q. Liu, J. Allen, R.N.C. Doig, J.R. Dahn, A guide to Ethylene carbonate-free electrolyte making for Li-Ion cells, J. Electrochem. Soc. 164 (2017) A5008–A5018, http://dx.doi.org/10.1149/2.0191701jes.
[11] P.G. Bruce, S.A. Freunberger, L.J. Hardwick, J.-M. Tarascon, Li–O2 and Li–S batteries with high energy storage, Nat. Mater. 11 (2012) 19–30, http://dx.doi.org/10.1038/NMAT3191.
[12] W.G. Zeier, J. Janek, A solid future for battery development, Nat. Inside Energy 1 (2016) 1–4, http://dx.doi.org/10.1038/nenergy.2016.141.
[13] J. Shi, Y. Liang, L. Li, Y. Peng, H. Yang, Evaluation of the electrochemical characteristics of silicon/lithium titanate composite as anode material for lithium ion batteries, Electrochim. Acta 155 (2015) 125–131, http://dx.doi.org/10.1016/j.electacta.2014.12.153.
[14] X. Shen, Z. Tian, R. Fan, L. Shao, D. Zhang, G. Cao, L. Kou, Y. Bai, Research progress on silicon/carbon composite anode materials for lithium-ion battery, J. Energy Chem. 0 (2018) 1–24, http://dx.doi.org/10.1016/j.jechem.2017.12.012.
[15] S. Chauque, F.Y. Oliva, A. Visintin, D. Barraco, E.P.M. Leiva, O.R. Cámara, Lithium titanate as anode material for lithium ion batteries: synthesis, post-treatment and its electrochemical response, J. Electroanal. Chem. 799 (2017) 142–155, http://dx.doi.org/10.1016/j.jelechem.2017.05.052.
[16] G. Xu, P. Han, S. Dong, H. Liu, G. Cui, L. Chen, Li4Ti5O12-based energy conversion and storage systems: status and prospects, Coord. Chem. Rev. 343 (2017) 139–184 https://doi.org/10.1016/j.ccr.2017.05.006.
[17] S.J. Moura, Techniques for Battery Health Conscious Power Management via Electrochemical Modeling and Optimal Control by, the University of Michigan,

(2011).
[18] S. Bashash, S.J. Moura, J.C. Forman, H.K. Fathy, Plug-in hybrid electric vehicle charge pattern optimization for energy cost and battery longevity, J. Power Sources 196 (2011) 541–549, http://dx.doi.org/10.1016/j.jpowsour.2010.07.001.
[19] W. Kempton, J. Tomić, Vehicle-to-grid power implementation: from stabilizing the grid to supporting large-scale renewable energy, J. Power Sources 144 (2005) 280–294, http://dx.doi.org/10.1016/j.jpowsour.2004.12.022.
[20] C. Liu, K.T. Chau, D. Wu, S. Gao, Opportunities and challenges of vehicle-to-home, vehicle-to-vehicle, and vehicle-to-grid technologies, Proc. IEEE 101 (2013) 2409–2427, http://dx.doi.org/10.1109/JPROC.2013.2271951.
[21] W. Kempton, J. Tomić, Vehicle-to-grid power fundamentals: calculating capacity and net revenue, J. Power Sources 144 (2005) 268–279, http://dx.doi.org/10.1016/j.jpowsour.2004.12.025.
[22] CPUC, 2017 Final RA Guide, (2017), pp. 1–44.
[23] J. Gannon, L. Chow, S. Brant, D. Brooks, CPUC: the 2013 – 2014 Resource Adequacy Report, (2015).
[24] P.B. Andersen, M. Marinelli, O.J. Olesen, C.A. Andersen, G. Poilasne, B. Christensen, O. Alm, The Nikola project intelligent electric vehicle integration, IEEE PES Innov. Smart Grid Technol. Conf. Eur, 2015, http://dx.doi.org/10.1109/ISGTEurope.2014.7028765.
[25] Ecoult, Grid-scale Energy Sources for Regulation Services Case Study: PJM Frequency Regulation, (2012).
[26] Argonne National Laboratory, Survey of U.S. Ancillary Services Markets, (2016).
[27] Lazard, Lazard's Levelized Cost of Storage Analysis - Version 1.0, (2015), http://dx.doi.org/10.1017/CBO9781107415324.004.
[28] Lazard, Lazard's Levelised Cost of Storage - Version 2.0, (2016), http://dx.doi.org/10.1080/14693062.2006.9685626.
[29] C. Eid, P. Codani, Y. Perez, J. Reneses, R. Hakvoort, Managing electric flexibility from Distributed Energy Resources: a review of incentives for market design, Renew. Sustain. Energy Rev. 64 (2016) 237–247, http://dx.doi.org/10.1016/j.rser.2016.06.008.
[30] P. Codani, Y. Perez, M. Petit, Financial shortfall for electric vehicles: economic impacts of Transmission System Operators market designs, Inside Energy 113 (2016) 422–431, http://dx.doi.org/10.1016/j.energy.2016.07.070.
[31] W. Kempton, V. Udo, K. Huber, K. Komara, S. Letendre, S. Baker, D. Brunner, N. Pearre, A Test of Vehicle-to-grid (V2G) for Energy Storage and Frequency Regulation in the PJM System, Newark, Delaware (2009).
[32] S. Vandael, T. Holvoet, G. Deconinck, S. Kamboj, W. Kempton, A comparison of two V2G mechanisms for providing ancillary services at the University of Delaware, Vancouver, Canada, 2013 IEEE Int. Conf. Smart Grid Commun, 2013, pp. 211–216.
[33] F.K. Tuffner, M. Kintner-Meyer, Using electric vehicles to mitigate imbalance requirements associated with an increased penetration of wind generation, IEEE Power Energy Soc. Gen. Meet, 2011, pp. 1–8, , http://dx.doi.org/10.1109/PES.2011.6039894.
[34] T. Markel, A. Meintz, K. Hardy, B. Chen, T. Bohn, J. Smart, D. Scoffield, R. Hovsapian, S. Saxena, J. Macdonald, S. Kiliccote, K. Kahl, R. Pratt, Multi-lab EV Smart Grid Integration Requirements Study, (2015) doi:NREL/TP-5400-63963.
[35] A. Meintz, T. Markel, M. Jun, J. Zhang, Integrating PEVs with renewables and the grid, IEEE Transp. Electrif. Conf. Expo, Dearborn, 2016, pp. 1–25 doi:NREL/PR-5500-66638.
[36] K.N. Kumar, B. Sivaneasan, P.H. Cheah, P.L. So, D.Z.W. Wang, V2G capacity estimation using dynamic EV scheduling, IEEE Trans. Smart Grid 5 (2014) 1051–1060, http://dx.doi.org/10.1109/TSG.2013.2279681.
[37] S.L. Koh, Y.S. Lim, Methodology for assessing viability of energy storage system for buildings, Inside Energy 101 (2016) 519–531, http://dx.doi.org/10.1016/j.energy.2016.02.047.
[38] G. Haines, A. McGordon, The simulation of vehicle-to-home systems - using electric vehicle battery storage to smooth domestic electricity demand, Proc. Ecol. Veh. Energies - EVRE, 2009, pp. 1–9 http://cmrt.centrale-marseille.fr/cpi/ever09/documents/papers/ev8/EVER09-paper-95.pdf.
[39] Pacific Gas and Electric Company, Economics of Power Factor Correction in Large facilities, > 400kW Electric Power basics, (2007), pp. 1–17 http://www.pge.com/includes/docs/pdfs/mybusiness/customerservice/energystatus/powerquality/powerfactor–revised-8-9-07.pdf.
[40] K.D. Slack, B.L. Capehart, Economic comparison of power factor correction by capacitors and high power factor/high-efficiency motors, Energy Eng. J. Assoc. Energy Eng. 95 (1998) 50–64, http://dx.doi.org/10.1080/01998595.1998.10530434.
[41] R.A. Verzijlbergh, M.D. Ilić, Z. Lukszo, The Role of Electric Vehicles on a green Island, NAPS 2011–43rd North Am. Power Symp, (2011), http://dx.doi.org/10.1109/NAPS.2011.6025199.
[42] J.D.K.K. Bishop, C.J. Axon, D. Bonilla, M. Tran, D. Banister, M.D. McCulloch, Evaluating the impact of V2G services on the degradation of batteries in PHEV and EV, Appl. Energy 111 (2013) 206–218, http://dx.doi.org/10.1016/j.apenergy.2013.04.094.
[43] S. Shinzaki, H. Sadano, Y. Maruyama, W. Kempton, Deployment of vehicle-to-grid technology and related issues, SAE Tech. Pap 01 (2015) 1–7, http://dx.doi.org/10.4271/2015-01-0306.
[44] D. Steward, Critical Elements of Vehicle-to-Grid (V2G) Economics, Strategic Partnership Project Report: NREL/TP-5400-69017 (2017) 1-12, September.
[45] M. Dubarry, A. Devie, K. McKenzie, Durability and reliability of electric vehicle batteries under electric utility grid operations: bidirectional charging impact analysis, J. Power Sources 358 (2017) 39–49, http://dx.doi.org/10.1016/j.jpowsour.2017.05.015.
[46] S. Han, S. Han, Economic feasibility of V2G frequency regulation in consideration of battery wear, Energies 6 (2013) 748–765, http://dx.doi.org/10.3390/en6020748.
[47] M. Doyle, T.F. Fuller, J. Newman, Modeling of galvanostatic charge and discharge of the lithium/polymer/insertion cell, J. Electrochem. Soc. 140 (1993) 1526–1533.
[48] G.-H. Kim, K. Smith, K.-J. Lee, S. Santhanagopalan, A. Pesaran, Multi-domain modeling of lithium-ion batteries encompassing multi-physics in varied length scales, J. Electrochem. Soc. 158 (2011), http://dx.doi.org/10.1149/1.3597614 A955.
[49] J. Wang, J. Purewal, P. Liu, J. Hicks-Garner, S. Soukiazian, E. Sherman, A. Sorenson, L. Vu, H. Tataria, M.W. Verbrugge, Degradation of lithium ion batteries employing graphite negatives and nickelecobaltemanganese oxide þ spinel manganese oxide positives: Part 1, aging mechanisms and life estimation, J. Power Sources 269 (2014) 937–948, http://dx.doi.org/10.1016/j.jpowsour.2014.07.028.
[50] K. Smith, M. Earleywine, E. Wood, J. Neubauer, A. Pesaran, Comparison of plug-in hybrid electric vehicle battery life across geographies and drive cycles, 2012 SAE World Congr. Exhib, 2012, http://dx.doi.org/10.4271/2012-01-0666.
[51] J. Wang, P. Liu, J. Hicks-Garner, E. Sherman, S. Soukiazian, M. Verbrugge, H. Tataria, J. Musser, P. Finamore, Cycle-life model for graphite-LiFePO4 cells, J. Power Sources 196 (2011) 3942–3948, http://dx.doi.org/10.1016/j.jpowsour.2010.11.134.
[52] K. Smith, G. Kim, T. Markel, A. Pesaran, Design of electric drive vehicle batteries for long life and low cost, IEEE 2010 Work. Accel. Stress Test. Reliab., Denver, Colorado, 2010, pp. 1–29 doi:NREL/PR-5400-48933.
[53] S. Grolleau, A. Delaille, H. Gualous, P. Gyan, R. Revel, J. Bernard, E. Redondo-Iglesias, J. Peter, Calendar aging of commercial graphite/LiFePO4 cell - predicting capacity fade under time dependent storage conditions, J. Power Sources 255 (2014) 450–458, http://dx.doi.org/10.1016/j.jpowsour.2013.11.098.
[54] P. Gyan, Calendar ageing modeling of lithium-ion batteries, Mat4Bat Summer Sch., La Rochelle, France, 2015, pp. 1–49, , http://dx.doi.org/10.1017/CBO9781107415324.004.
[55] P. Gyan, P. Aubret, J. Hafsaoui, F. Sellier, S. Bourlot, S. Zinola, F. Badin, Experimental assessment of battery cycle life within the SIMSTOCK research program, Oil Gas Sci. Technol. D Ifp Energies Nouv 68 (2013) 137–147, http://dx.doi.org/10.2516/ogst/2013106.
[56] A. Fotouhi, D.J. Auger, K. Propp, S. Longo, M. Wild, A review on electric vehicle battery modelling: from Lithium-ion toward Lithium-Sulphur, Renew. Sustain. Energy Rev. 56 (2016) 1008–1021, http://dx.doi.org/10.1016/j.rser.2015.12.009.
[57] W. Waag, C. Fleischer, D.U. Sauer, Critical review of the methods for monitoring of lithium-ion batteries in electric and hybrid vehicles, J. Power Sources 258 (2014) 321–339, http://dx.doi.org/10.1016/j.jpowsour.2014.02.064.
[58] C. Zhang, K. Li, S. McLoone, Z. Yang, Battery modelling methods for electric vehicles - a Review, 2014 Eur. Control Conf, 2014, pp. 2673–2678, , http://dx.doi.org/10.1109/ECC.2014.6862541.
[59] A. Barré, B. Deguilhem, S. Grolleau, M. Gérard, F. Suard, D. Riu, A review on lithium-ion battery ageing mechanisms and estimations for automotive applications, J. Power Sources 241 (2013) 680–689, http://dx.doi.org/10.1016/j.jpowsour.2013.05.040 Review.
[60] M. Dubarry, C. Truchot, B.Y. Liaw, Synthesize battery degradation modes via a diagnostic and prognostic model, J. Power Sources 219 (2012) 204–216, http://dx.doi.org/10.1016/j.jpowsour.2012.07.016.
[61] A.J. Bard, L.R. Faulkner, Electrochemical Methods: Fundamentals and Applications, second ed., John Wiley & Sons, Inc., New York, 2001, http://dx.doi.org/10.1016/B978-0-12-381373-2.00056-9.
[62] J. Garcia Villalobos, Optimized Charging Control Method for Plug-in Eelectric Vehicles in LV Distribution Networks, Universidad Del Pais Vasco, 2016, pp. 1–230.
[63] X. Zuo, J. Zhu, P. Müller-Buschbaum, Y.-J. Cheng, Silicon based lithium-ion battery anodes: a chronicle perspective review, Nanomater. Energy 31 (2017) 113–143, http://dx.doi.org/10.1016/j.nanoen.2016.11.013.
[64] E. Ignatev, Performance Degradation Modelling and Techno- Economic Analysis of Lithium-ion Battery Energy, Lappeenranta University of Technology, 2016.
[65] G. Seckmeyer, A. Zittermann, R. Mckenzie, Encyclopedia of Sustainability Science and Technology, (2012), http://dx.doi.org/10.1007/978-1-4419-0851-3.
[66] M. Park, X. Zhang, M. Chung, G.B. Less, A.M. Sastry, A review of conduction phenomena in Li-ion batteries, J. Power Sources 195 (2010) 7904–7929, http://dx.doi.org/10.1016/j.jpowsour.2010.06.060.
[67] M. Broussely, S. Herreyre, P. Biensan, P. Kasztejna, K. Nechev, R.J. Staniewicz, Aging mechanism in Li ion cells and calendar life predictions, J. Power Sources (2001) 97–98, http://dx.doi.org/10.1016/S0378-7753(01)00722-4 13–21.
[68] M.R. Palacín, A. De Guibert, Batteries: why do batteries fail? Science (Wash. D C) 351 (2016), http://dx.doi.org/10.1126/science.1253292.
[69] A.J. Gmitter, I. Plitz, G.G. Amatucci, High concentration dinitrile, 3-alkoxypropionitrile, and linear carbonate electrolytes enabled by vinylene and monofluoroethylene carbonate additives, J. Electrochem. Soc. 159 (2012), http://dx.doi.org/10.1149/2.016204jes A370.
[70] A. Yoshino, Development of the lithium-ion battery and recent technological trends, Lithium-Ion Batter. Adv. Appl, 2014, pp. 1–20, , http://dx.doi.org/10.1016/B978-0-444-59513-3.00001-7.
[71] A.J. Smith, J.C. Burns, S. Trussler, J.R. Dahn, Precision measurements of the coulombic efficiency of lithium-ion batteries and of electrode materials for lithium-ion batteries, J. Electrochem. Soc. 157 (2010), http://dx.doi.org/10.1149/1.3268129 A196.
[72] C.J. Orendorff, The role of separators in lithium-ion cell safety, Interface Mag 21 (2012) 61–65, http://dx.doi.org/10.1149/2.F07122if.

[73] S.S. Zhang, A review on the separators of liquid electrolyte Li-ion batteries, J. Power Sources 164 (2007) 351–364, http://dx.doi.org/10.1016/j.jpowsour.2006.10.065.
[74] Sandia National Labs, Sandia National labs, sandia transp. Res. Proj. Funded as a Part DOE's "EV everywhere" funding progr, (2014) http://energy.sandia.gov/sandia-transportation-energy-research-project-funded-as-a-part-of-does-ev-everywhere-funding-program/ , Accessed date: 22 March 2018.
[75] J. Vetter, P. Novak, M.R. Wagner, C. Veit, K.C. Moller, J.O. Besenhard, M. Winter, M. Wohlfahrt-Mehrens, C. Vogler, A. Hammouche, Ageing mechanisms in lithium-ion batteries, J. Power Sources 147 (2005) 269–281, http://dx.doi.org/10.1016/j.jpowsour.2005.01.006.
[76] C. Schlasza, P. Ostertag, D. Chrenko, R. Kriesten, D. Bouquain, Review on the aging mechanisms in Li-ion batteries for electric vehicles based on the FMEA method, 2014 IEEE Transp. Electrif. Conf. Expo, 2014, pp. 1–6, , http://dx.doi.org/10.1109/ITEC.2014.6861811.
[77] T.R. Tanim, M.G. Shirk, R.L. Bewley, E.J. Dufek, B.Y. Liaw, Fast charge implications: pack and cell analysis and comparison, J. Power Sources 381 (2018) 56–65, http://dx.doi.org/10.1016/j.jpowsour.2018.01.091.
[78] L. Lu, X. Han, J. Li, J. Hua, M. Ouyang, A review on the key issues for lithium-ion battery management in electric vehicles, J. Power Sources 226 (2013) 272–288, http://dx.doi.org/10.1016/j.jpowsour.2012.10.060.
[79] J. Neubauer, K. Smith, E. Wood, A. Pesaran, J. Neubauer, K. Smith, E. Wood, A. Pesaran, Identifying and Overcoming Critical Barriers to Widespread Second Use of PEV Batteries, (2015) doi:NREL/TP-5400-63332.
[80] J.S. Neubauer, A. Pesaran, B. Williams, M. Ferry, J. Eyer, A techno-economic analysis of PEV battery second use: repurposed-battery selling price and commercial and industrial end-user value, SAE Int (2012), http://dx.doi.org/10.4271/2012-01-0349.
[81] K. Smith, C.-Y. Wang, Power and thermal characterization of a lithium-ion battery pack for hybrid-electric vehicles, J. Power Sources 160 (2006) 662–673, http://dx.doi.org/10.1016/j.jpowsour.2006.01.038.
[82] S. Saxena, C. Le Floch, J. Macdonald, S. Moura, Quantifying EV battery end-of-life through analysis of travel needs with vehicle powertrain models, J. Power Sources 282 (2015) 265–276, http://dx.doi.org/10.1016/j.jpowsour.2015.01.072.
[83] S.J. An, J. Li, C. Daniel, D. Mohanty, S. Nagpure, D.L. Wood, The State of Understanding of the Lithium-ion-battery Graphite Solid Electrolyte Interphase (SEI) and its Relationship to Formation Cycling, Carbon N. Y vol. 105, (2016), pp. 52–76, http://dx.doi.org/10.1016/j.carbon.2016.04.008.
[84] E. Prada, D. Di Domenico, Y. Creff, J. Bernard, V. Sauvant-moynot, F. Huet, A simplified electrochemical and thermal aging model of LiFePO 4 -graphite Li-ion Batteries : power and capacity fade simulations, J. Electrochem. Soc. 160 (2013) A616–A628, http://dx.doi.org/10.1149/2.053304jes.
[85] K. Uddin, S. Perera, W. Widanage, L. Somerville, J. Marco, Characterising lithium-ion battery degradation through the identification and tracking of electrochemical battery model parameters, Batteries 2 (2016) 13, http://dx.doi.org/10.3390/batteries2020013.
[86] K.A. Smith, Electrochemical Modeling, Estimation and Control of Lithium Ion Batteries, The Pennsylvania State University, 2006.
[87] K. Uddin, T. Jackson, W.D. Widanage, G. Chouchelamane, P.A. Jennings, J. Marco, On the possibility of extending the lifetime of lithium-ion batteries through optimal V2G facilitated by an integrated vehicle and smart-grid system, Inside Energy 133 (2017) 710–722, http://dx.doi.org/10.1016/j.energy.2017.04.116.
[88] M. Ben-Marzouk, A. Chaumond, E. Redondo-Iglesias, M. Montaru, S. Pelissier, Experimental protocols and first results of calendar and/or cycling aging study of lithium-ion batteries - the MOBICUS project, 29th World Electr. Veh. Symp. Exhib. (EVS 29), Montreal, Canada, 2016, pp. 388–397.
[89] C. Lin, A. Tang, H. Mu, W. Wang, C. Wang, Aging mechanisms of electrode materials in lithium-ion batteries for electric vehicles, J. Chem. 2015 (2015) 1–11, http://dx.doi.org/10.1155/2015/104673.
[90] H. Ribberink, K. Darcovich, F. Pincet, Battery life impact of vehicle-to-grid application of electric vehicles, EVS28, Int. Electr. Veh. Symp. Exhib (2015) 1–11.
[91] K. Smith, E. Wood, S. Santhanagopalan, G. Kim, A. Pesaran, Advanced models and controls for prediction and extension of battery lifetime, Large Lithium Ion Batter. Technol. Appl. Symp. Adv. Automot. Batter. Conf., Atlanta, Georgia, 2014 doi:NREL/PR-5400-61037.
[92] A. Delaille, S. Grolleau, F. Duclaud, SIMCAL Project: calendar aging results obtained on a panel of 6 commercial Li-ion cells, Electrochem. Energy Summit l'Electrochemical Soc. 101 (2013) doi:hal-00920366.
[93] J. Hall, T. Lin, G. Brown, P. Biensan, F. Bonhomme, Decay Processes, Life Predictions, For lithium ion satellite cells, 4th Int. Energy Convers. Eng. Conf. Exhib, American Institute of Aeronautics and Astronautics, San Diego, 2006, pp. 1–11, , http://dx.doi.org/10.2514/6.2006-4078.
[94] M. Broussely, Aging of Li-ion batteries and life prediction, an update, 3rd Int. Symp. Large Li-Ion Batter. Technol. Appl., Long Beach, California, 2007.
[95] K. Smith, T. Markel, A. Pesaran, PHEV battery trade-off study and standby thermal control, 26th Int. Batter. Semin. Exhib., Fort Lauderdale, Florida, 2009, pp. 1–30 doi:NREL/PR-540-45048.
[96] K. Smith, C.Y. Wang, Solid-state diffusion limitations on pulse operation of a lithium ion cell for hybrid electric vehicles, J. Power Sources 161 (2006) 628–639, http://dx.doi.org/10.1016/j.jpowsour.2006.03.050.
[97] K. Smith, M. Earleywine, E. Wood, A. Pesaran, Battery wear from disparate duty-cycles: opportunities for electric-drive vehicle battery health management, Am. Control Conf (2012) 9 doi:NREL/CP-5400-54698.
[98] J. Wang, P. Liu, J. Hicks-Garner, E. Sherman, S. Soukiazian, M. Verbrugge, H. Tataria, J. Musser, P. Finamore, Cycle-life model for graphite-LiFePO4 cells, J. Power Sources 196 (2011) 3942–3948, http://dx.doi.org/10.1016/j.jpowsour.2010.11.134.
[99] A. Delaille, Calendar ageing of Li-ion batteries : results from ageing tests and understanding from autopsies, Mat4Bat Summer Sch., La Rochelle, France, 2015, pp. 1–36.
[100] I. Baghdadi, O. Briat, P. Gyan, J. Michel, State of health assessment for lithium batteries based on voltage – time relaxation measure, Electrochim. Acta 194 (2016) 461–472, http://dx.doi.org/10.1016/j.electacta.2016.02.109.
[101] USABC, Appendix a: Generic Test Plan Outline for USABC Battery Testing, (2014).
[102] D.C. Robertson, J.P. Christophersen, T. Bennett, L.K. Walker, F. Wang, S. Liu, B. Fan, I. Bloom, A comparison of battery testing protocols: those used by the U.S. advanced battery consortium and those used in China, J. Power Sources 306 (2016) 268–273, http://dx.doi.org/10.1016/j.jpowsour.2015.12.004.
[103] A. Hoke, A. Brissette, A. Pratt, K. Smith, Electric vehicle charge optimization including effects of lithium-ion battery degradation, IEEE Veh. Power Propuls. Conf, 2011, http://dx.doi.org/10.1109/VPPC.2011.6043046.
[104] D. Wang, J. Coignard, T. Zeng, C. Zhang, S. Saxena, Quantifying electric vehicle battery degradation from driving vs. vehicle-to-grid services, J. Power Sources 332 (2016) 193–203, http://dx.doi.org/10.1016/j.jpowsour.2016.09.116.
[105] J. Neubauer, E. Wood, Thru-life impacts of driver aggression, climate, cabin thermal management, and battery thermal management on battery electric vehicle utility, J. Power Sources 259 (2014) 262–275, http://dx.doi.org/10.1016/j.jpowsour.2014.02.083.
[106] S. Saxena, J. Macdonald, D. Black, S. Kiliccote, Quantifying the flexibility for electric vehicles to offer demand response to reduce grid impacts without compromising individual driver mobility needs, SAE Tech. Pap. 2015–April, 2015, http://dx.doi.org/10.4271/2015-01-0304.
[107] P. Siano, Demand response and smart grids - a survey, Renew. Sustain. Energy Rev. 30 (2014) 461–478, http://dx.doi.org/10.1016/j.rser.2013.10.022.
[108] M. Petit, E. Prada, V. Sauvant-Moynot, Development of an empirical aging model for Li-ion batteries and application to assess the impact of Vehicle-to-Grid strategies on battery lifetime, Appl. Energy 172 (2016) 398–407, http://dx.doi.org/10.1016/j.apenergy.2016.03.119.
[109] J. Fluhr, K.H. Ahlert, C. Weinhardt, A stochastic model for simulating the availability of electric vehicles for services to the power grid, Proc. Annu. Hawaii Int. Conf. Syst. Sci, 2010, pp. 1–10, , http://dx.doi.org/10.1109/HICSS.2010.33.
[110] Q. Wu, A.H. Nielsen, J. Ostergaard, S.T. Cha, F. Marra, Y. Chen, C. Træholt, Driving pattern analysis for electric vehicle (EV) grid integration study, 2010 IEEE PES Innov. Smart Grid Technol. Conf. Eur. (ISGT Eur, 2010, pp. 1–6, , http://dx.doi.org/10.1109/ISGTEUROPE.2010.5751581.
[111] J. Neubauer, Battery Lifetime Analysis and Simulation Tool (BLAST) Documentation, (2014) doi:NREL/TP-5400-63246.
[112] L. Fournie, C. Andrey, J. Hentschel, G. Wilkinson, Integration of Electricity Balancing Markets and Regional Procurement of Balancing Reserves, (2016), http://dx.doi.org/10.2832/463464.

Glossary

Ah: Amp-hour
B2L: Battery Second Life
BESS: Battery Energy Storage Systems
BMS: Battery Management System
CCGT: Combined Cycle and Gas Turbine
C-rate: Charge Rate
DER: Distributed Energy Resource
DoD: Depth of Discharge
EC: Ethylene Carbonate
ECM: Equivalent Circuit Model
EIS: Electrochemical Impedance Spectroscopy
EMC: Ethel Methyl Carbonate
EoL: End of Life
EV: Electric Vehicle
FCEV: Fuel Cell Electric Vehicle
G: Graphite
HPPC: Hybrid Pulse Power Characterization
HV: High Voltage Network
ICE: Internal Combustion Engine
LAM: Loss of Active Material
LCOS: Levelized Cost of Storage
LCP: Lithium Cobalt Phosphate
LFP: Lithium Iron Phosphate
LFSF: Lithium Iron Fluorosulfate
$LiBF_4$: Lithium Tetrafluoroborate
Li-O2: Lithium Air
$LiPF_6$: Lithium Hexafluorophosphate
Li-S: Lithium Sulfur
LLI: Loss of Lithium Inventory
LMO: Lithium Manganese Oxide
LMO-NMC: Manganese Oxide/Nickle-Manganese-Cobalt blend
LNO: Lithium Nickel Oxide
LTO: Lithium Titanate Oxide
LTS: Lithium Titanium Sulfide
LV: Low Voltage Network
MOBICUS: Modeling of Batteries Including the Coupling between Calendar and Usage Aging
MV: Medium Voltage Network

NCA: Nickel Cobalt Aluminum Oxide
NCM or NMC: Nickel Cobalt Manganese
NPV: Net Present Value
NREL: National Renewable Energy Laboratory
OCV: Open Circuit Voltage
PHEV: Plug-in Hybrid Electric Vehicle
PJM: PJM Wholesale Energy Market Operator
PVT: Present Value of Throughput
SEI: Solid Electrolyte Interface
SOC: State of Charge
SOH: State of Health
SSB: Solid State Battery
TCO: Total Cost of Ownership
V2B: Vehicle-to-Building
V2G: Vehicle-to-Grid
V2H: Vehicle-to-Load
V2V: Vehicle-to-Vehicle
V2X: Vehicle-to-Anything